

REFERENCES

- 7.1. Bollay W. "Aerodynamic Stability and Automatic Control." *Journal of the Aeronautical Sciences* 18, no. 9 (1951), pp. 569–617.
 - 7.2. Raven, F. H. *Automatic Control Engineering*. New York: McGraw-Hill, 1995.
 - 7.3. Kuo, B. C. *Automatic Control Systems*. Englewood Cliffs, NJ: Prentice-Hall, 1975.
 - 7.4. Shinners, S. M. *Modern Control System Theory and Application*. Reading, MA: Addison Wesley, 1978.
 - 7.5. D'Souza, A. F. *Design of Control Systems*. Englewood Cliffs, NJ: Prentice-Hall, 1988.
 - 7.6. Hale, F. J. *Introduction to Control System Analysis and Design*. Englewood Cliffs, NJ: Prentice-Hall, 1988.
 - 7.7. Nagrath, I. J.; and M. Gopal. *Control Systems Engineering*. New York: John Wiley and Sons, 1975.

CHAPTER 8

Application of Classical Control Theory to Aircraft Autopilot Design

"The application of automatic control systems to aircraft promises to bring about the most important new advances in aeronautics in the future."

William Bollay, 14th Wright Brothers Lecture, 1950

8.1 INTRODUCTION

The rapid advancement of aircraft design from the very limited capabilities of the Wright brothers' first successful airplane to today's high performance military, commercial, and general aviation aircraft required the development of many technologies: aerodynamics, structures, materials, propulsion, and flight controls. Today's aircraft designs rely heavily on automatic control systems to monitor and control many of the aircraft's subsystems.

The development of automatic control systems has played an important role in the growth of civil and military aviation. Modern aircraft include a variety of automatic control systems that aid the flight crew in navigation, flight management, and augmenting the stability characteristics of the airplane. In this chapter we use control theory to design simple autopilots that can be used by the flight crew to lessen their workload during cruising and help them land their aircraft during adverse weather conditions. In addition, we also discuss how automatic control systems can be used to provide artificial stability to improve the flying qualities of an airplane.

Table 8.1 lists some of the functions that automatic control systems provide for flight control. In addition to the automatic flight control system, modern aircraft use control systems to aid in the navigation of the aircraft.

The development of autopilots closely followed the successful development of a powered, human-carrying airplane by the Wright brothers. In 1914 the Sperry brothers demonstrated the first successful autopilot. The autopilot was capable of maintaining pitch, roll, and heading angles. To demonstrate the effectiveness of their design, Lawrence Sperry trimmed his airplane for straight and level flight and then engaged the autopilot. He then proceeded to stand in the cockpit with his hands raised above his head while his mechanic walked out along the wings in an

TABLE 8.1
Automatic flight control system

Flight control system to reduce pilot workload
Attitude control systems to maintain pitch, roll, or heading
Altitude hold control system to maintain a desired altitude
Speed control system to maintain a constant speed or Mach number
Stability augmentation systems
If an airplane is marginally stable or unstable, automatic control systems can provide proper flight vehicle stability
Automatic control can be used to ensure an airplane has the appropriate handling qualities; additional damping is incorporated by using a roll, pitch, or yaw damper
Landing aids
A glide slope control system to guide the airplane down an electronic beam to the runway
A localizer to align the aircraft in the lateral direction with the runway centerline as the airplane descends down the glide slope
A flare control system that helps the aircraft make the transition from the glide slope to the runway

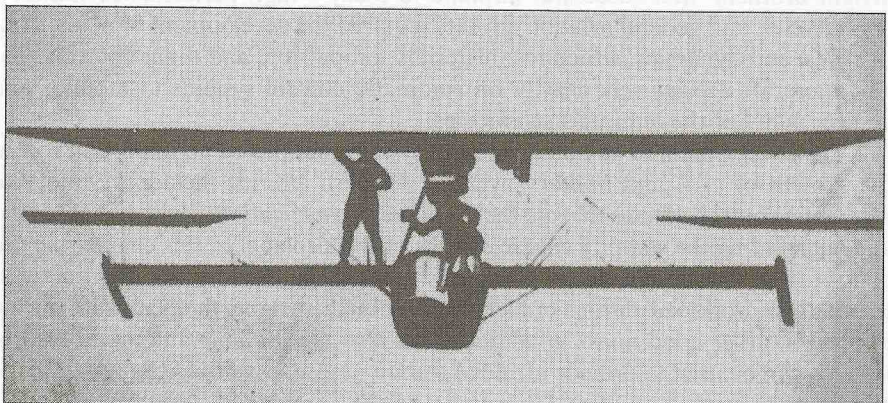


FIGURE 8.1
Sperry's flight demonstration of a three-axis automatic control system (from [8.1]).

attempt to upset the airplane's equilibrium. Figure 8.1 shows a photograph of the remarkable flight. The autopilot provided aileron, rudder, and elevator commands so that the airplane remained in a wings-level attitude.

8.2 AIRCRAFT TRANSFER FUNCTIONS

The longitudinal and lateral equations of motion were described by a set of linear differential equations in Chapter 3. A very useful concept in the analysis and design of control systems is the transfer function. The transfer function gives the relationship between the output of and input to a system. In the case of aircraft dynamics it specifies the relationship between the motion variables and the control input. The transfer function is defined as the ratio of the Laplace transform of the output to the Laplace transform of the input with all the initial conditions set to 0. (i.e., the system is assumed to be initially in equilibrium). For the reader who is not familiar with theory of Laplace transformations, a brief review of the basic concepts of Laplace transformation theory is included in Appendix C at the end of this book. In the following sections we develop the transfer function based on the longitudinal and lateral approximations developed in Chapters 4 and 5. We develop these simpler mathematical models so that we can examine the idea behind various autopilots without undue mathematical complexity.

8.2.1 Short-Period Dynamics

In Chapter 4 the equations for the short-period motions were developed for the case where the control was held fixed. The equation with control input from the elevator in state space form can be written as

$$\begin{bmatrix} \Delta\dot{\alpha} \\ \Delta\dot{q} \end{bmatrix} = \begin{bmatrix} Z_\alpha/u_0 & 1 \\ M_\alpha + M_{\dot{\alpha}}Z_\alpha/u_0 & M_q + M_{\dot{q}} \end{bmatrix} \begin{bmatrix} \Delta\alpha \\ \Delta q \end{bmatrix} + \begin{bmatrix} Z_{\delta_e}/u_0 \\ M_{\delta_e} + M_{\dot{\alpha}}Z_{\delta_e}/u_0 \end{bmatrix} [\Delta\delta_e] \quad (8.1)$$

The control due to the propulsion system is neglected here for simplicity. Taking the Laplace transform of this equation yields

$$(s - Z_\alpha/u_0) \Delta\alpha(s) - \Delta q(s) = Z_{\delta_e}/u_0 \Delta\delta_e(s) \quad (8.2)$$

$$-(M_\alpha + M_{\dot{\alpha}}Z_\alpha/u_0) \Delta\alpha(s) + [s - (M_q + M_{\dot{q}})] \Delta q(s) = (M_{\delta_e} + M_{\dot{\alpha}}Z_{\delta_e}/u_0) \Delta\delta_e \quad (8.3)$$

If we divide these equations by $\Delta\delta_e(s)$ we obtain a set of algebraic equations in terms of the transfer functions $\Delta\alpha(s)/\Delta\delta_e(s)$ and $\Delta q(s)/\Delta\delta_e(s)$:

$$(s - Z_\alpha/u_0) \frac{\Delta\alpha(s)}{\Delta\delta_e(s)} - \frac{\Delta q(s)}{\Delta\delta_e(s)} = Z_{\delta_e}/u_0 \quad (8.4)$$

$$-(M_\alpha + M_{\dot{\alpha}} Z_\alpha/u_0) \frac{\Delta\alpha(s)}{\Delta\delta_e(s)} + [s - (M_q + M_{\dot{\alpha}})] \frac{\Delta q(s)}{\Delta\delta_e(s)} = M_{\delta_e} + M_{\dot{\alpha}} \frac{Z_{\delta_e}}{u_0} \quad (8.5)$$

Solving for $\Delta\alpha(s)/\Delta\delta_e(s)$ and $\Delta q(s)/\Delta\delta_e(s)$ by Cramer's rule yields

$$\frac{\Delta\alpha(s)}{\Delta\delta_e(s)} = \frac{N_{\delta_e}^\alpha(s)}{\Delta_{sp}(s)} = \frac{\begin{vmatrix} Z_{\delta_e}/u_0 & -1 \\ M_{\delta_e} + M_{\dot{\alpha}} Z_{\delta_e}/u_0 & s - (M_q + M_{\dot{\alpha}}) \end{vmatrix}}{\begin{vmatrix} s - Z_\alpha/u_0 & -1 \\ -(M_\alpha + M_{\dot{\alpha}} Z_\alpha/u_0) & s - (M_q + M_{\dot{\alpha}}) \end{vmatrix}} \quad (8.6)$$

When expanded, the numerator and denominator are polynomials in the Laplace variable s . The coefficients of the polynomials are a function of the stability derivatives. McRuer, Ashkenas, and Graham [8.2] use a shorthand notation to express the transfer function polynomials. We will use this convenient notation to present the transfer function developed here. An example of the notation follows:

$$\frac{\Delta\alpha(s)}{\Delta\delta_e(s)} = \frac{N_{\delta_e}^\alpha(s)}{\Delta_{sp}(s)} = \frac{A_\alpha s + B_\alpha}{As^2 + Bs + C} \quad (8.7)$$

where the coefficients in the numerator and denominator are given in Table 8.2. The transfer function for the change in pitch rate to the change in elevator angle can be shown to be

$$\frac{\Delta q(s)}{\Delta\delta_e(s)} = \frac{N_{\delta_e}^q(s)}{\Delta_{sp}(s)} = \frac{\begin{vmatrix} s - Z_\alpha/u_0 & Z_{\delta_e}/u_0 \\ -(M_\alpha + M_{\dot{\alpha}} Z_\alpha/u_0) & M_{\delta_e} + M_{\dot{\alpha}} Z_{\delta_e}/u_0 \end{vmatrix}}{\begin{vmatrix} s - Z_\alpha/u_0 & -1 \\ -(M_\alpha + M_{\dot{\alpha}} Z_\alpha/u_0) & s - (M_q + M_{\dot{\alpha}}) \end{vmatrix}} \quad (8.8)$$

or

$$\frac{\Delta q(s)}{\Delta\delta_e(s)} = \frac{N_{\delta_e}^q(s)}{\Delta_{sp}(s)} = \frac{A_q s + B_q}{As^2 + Bs + C} \quad (8.9)$$

Again the coefficients of the polynomials are defined in Table 8.2.

TABLE 8.2
Short-period transfer function approximations

	A, A_α , or A_q	B, B_α , or B_q	C
$\Delta_{sp}(s)$	1	$-(M_q + M_{\dot{\alpha}} + Z_\alpha/u_0)$	$Z_\alpha M_q/u_0 - M_\alpha$
$N_{\delta_e}^\alpha(s)$	Z_{δ_e}/u_0	$M_{\delta_e} - M_q Z_{\delta_e}/u_0$	
$N_{\delta_e}^q(s)$	$M_{\delta_e} + M_{\dot{\alpha}} Z_{\delta_e}/u_0$	$M_\alpha Z_{\delta_e}/u_0 - M_{\delta_e} Z_\alpha/u_0$	

8.2.2 Long-Period or Phugoid Dynamics

The state-space equation for the long period or phugoid approximation are as follows:

$$\begin{bmatrix} \Delta\dot{u} \\ \Delta\dot{\theta} \end{bmatrix} = \begin{bmatrix} X_u & -g \\ -\frac{Z_u}{u_0} & 0 \end{bmatrix} \begin{bmatrix} \Delta u \\ \Delta\theta \end{bmatrix} + \begin{bmatrix} X_{\delta_e} & X_{\delta_T} \\ -\frac{Z_{\delta_e}}{u_0} & -\frac{Z_{\delta_T}}{u_0} \end{bmatrix} \begin{bmatrix} \Delta\delta_e \\ \Delta\delta_T \end{bmatrix} \quad (8.10)$$

The Laplace transformation of the approximate equations for the long period are

$$(s - X_u) \Delta u(s) + g \Delta\theta(s) = X_{\delta_e} \Delta\delta_e(s) + X_{\delta_T} \Delta\delta_T(s) \quad (8.11)$$

$$\frac{Z_u}{u_0} \Delta u(s) + s \Delta\theta(s) = -\frac{Z_{\delta_e}}{u_0} \Delta\delta_e(s) - \frac{Z_{\delta_T}}{u_0} \Delta\delta_T(s) \quad (8.12)$$

The transfer function $\Delta u(s)/\Delta\delta_e(s)$ and $\Delta\theta(s)/\Delta\delta_e(s)$ can be found by setting $\Delta\delta_T(s)$ to 0 and solving for the appropriate transfer function as follows:

$$(s - X_u) \frac{\Delta u(s)}{\Delta\delta_e(s)} + g \frac{\Delta\theta(s)}{\Delta\delta_e(s)} = X_{\delta_e} \quad (8.13)$$

$$\frac{Z_u}{u_0} \frac{\Delta u(s)}{\Delta\delta_e(s)} + s \frac{\Delta\theta(s)}{\Delta\delta_e(s)} = -\frac{Z_{\delta_e}}{u_0} \quad (8.14)$$

The equations of motion have been reduced to a set of algebraic equations in terms of the desired transfer function. These equations can be solved to yield the transfer functions

$$\frac{\Delta u(s)}{\Delta\delta_e(s)} = \begin{vmatrix} X_{\delta_e} & g \\ -\frac{Z_{\delta_e}}{u_0} & s \end{vmatrix} \quad (8.15)$$

$$\frac{\Delta u(s)}{\Delta\delta_e(s)} = \frac{X_{\delta_e}s + gZ_{\delta_e}/u_0}{s^2 + X_us - \frac{Z_u g}{u_0}} \quad (8.16)$$

In a similar manner $\Delta\theta(s)/\Delta\delta(s)$ can be shown to be

$$\frac{\Delta\theta(s)}{\Delta\delta_e(s)} = \frac{-\frac{Z_{\delta_e}}{u_0}s + \left(\frac{X_u Z_{\delta_e}}{u_0} - \frac{Z_u X_{\delta_e}}{u_0}\right)}{s^2 - X_us - \frac{Z_u g}{u_0}} \quad (8.17)$$

TABLE 8.3
Long-period transfer function approximations

A, A_u , or A_θ	B, B_u , or B_θ	C
$\Delta_p(s)$	1	$-X_u$
$N_{\delta_e}^u(s)$	X_{δ_e}	gZ_{δ_e}/u_0
$N_{\delta_e}^\theta(s)$	$-Z_{\delta_e}/u_0$	$X_u Z_{\delta_e}/u_0 - Z_u X_{\delta_e}/u_0$

The transfer functions can be written in a symbolic form in the following manner:

$$\frac{\Delta u(s)}{\Delta \delta_e(s)} = \frac{N_{\delta_e}^u(s)}{\Delta_p(s)} = \frac{A_u s + B_u}{As^2 + Bs + C} \quad (8.18)$$

$$\frac{\Delta \theta(s)}{\Delta \delta_e(s)} = \frac{N_{\delta_e}^\theta(s)}{\Delta_p(s)} = \frac{A_\theta s + B_\theta}{As^2 + Bs + C} \quad (8.19)$$

where A_u , B_u , and so forth are defined in Table 8.3. The transfer functions for the propulsive control, that is, $\Delta u(s)/\Delta \delta_T(s)$ and $\Delta \theta(s)/\Delta \delta_T(s)$, have the same form except that the derivatives with respect to δ_e are replaced by derivatives with respect to δ_T . Therefore, Table 8.3 can be used for both aerodynamic and propulsive control transfer functions provided that the appropriate control derivatives are used.

8.2.3 Roll Dynamics

The equation of motion for a pure rolling motion, developed in Chapter 5, is

$$\Delta \dot{p} - L_p \Delta p = L_{\delta_a} \Delta \delta_a \quad (8.20)$$

The transfer function $\Delta p(s)/\Delta \delta_a(s)$ and $\Delta \phi(s)/\Delta \delta_a(s)$ can be obtained by taking the Laplace transform of the roll equation:

$$(s - L_p) \Delta p(s) = L_{\delta_a} \Delta \delta_a(s) \quad (8.21)$$

or

$$\frac{\Delta p(s)}{\Delta \delta_a(s)} = \frac{L_{\delta_a}}{s - L_p} \quad (8.22)$$

But the roll rate Δp is defined as $\Delta \dot{\phi}$; therefore,

$$\Delta p(s) = s \Delta \phi(s) \quad (8.23)$$

or

$$\frac{\Delta \phi(s)}{\Delta \delta_a(s)} = \frac{L_{\delta_a}}{s(s - L_p)} \quad (8.24)$$

8.2.4 Dutch Roll Approximation

The final simplified transfer function we will develop is for the Dutch roll motion. The approximate equations can be shown to be

$$\begin{bmatrix} \Delta \beta \\ \Delta r \end{bmatrix} = \begin{bmatrix} Y_\beta/u_0 & -(1 - Y_r/u_0) \\ N_\beta & N_r \end{bmatrix} \begin{bmatrix} \Delta \beta \\ \Delta r \end{bmatrix} + \begin{bmatrix} Y_{\delta_r}/u_0 & 0 \\ N_{\delta_r} & N_{\delta_a} \end{bmatrix} \begin{bmatrix} \Delta \delta_r \\ \Delta \delta_a \end{bmatrix} \quad (8.25)$$

Taking the Laplace transform and rearranging yields

$$(s - Y_\beta/u_0) \Delta \beta(s) + (1 - Y_r/u_0) \Delta r(s) = Y_{\delta_r}/u_0 \Delta \delta_r(s) \quad (8.26)$$

$$-N_\beta \Delta \beta(s) + (s - N_r) \Delta r(s) = N_{\delta_a} \Delta \delta_a(s) + N_{\delta_r} \Delta \delta_r(s) \quad (8.27)$$

The transfer functions $\Delta \beta(s)/\Delta \delta_r(s)$, $\Delta r(s)/\Delta \delta_r(s)$, $\Delta \beta(s)/\Delta \delta_a(s)$, and $\Delta r(s)/\Delta \delta_a(s)$ can be obtained by setting $\Delta \delta_a(s)$ to 0 and solving for $\Delta \beta(s)/\Delta \delta_r(s)$ and $\Delta r(s)/\Delta \delta_r(s)$. Next set $\Delta \delta_r(s)$ equal to 0 and solve for $\Delta \beta(s)/\Delta \delta_a(s)$ and $\Delta r(s)/\Delta \delta_a(s)$. The transfer functions $\Delta \beta(s)/\Delta \delta_a(s)$ and $\Delta r(s)/\Delta \delta_a(s)$ are obtained as follows:

$$(s - Y_\beta/u_0) \frac{\Delta \beta(s)}{\Delta \delta_r(s)} + (1 - Y_r/u_0) \frac{\Delta r(s)}{\Delta \delta_r(s)} = Y_{\delta_r}/u_0 \quad (8.28)$$

$$-N_\beta \frac{\Delta \beta(s)}{\Delta \delta_r(s)} + (s - N_r) \frac{\Delta r(s)}{\Delta \delta_r(s)} = N_{\delta_r} \quad (8.29)$$

Solving for the transfer function yields

$$\frac{\Delta \beta(s)}{\Delta \delta_r(s)} = \frac{\begin{vmatrix} Y_{\delta_r}/u_0 & 1 - Y_r/u_0 \\ N_{\delta_r} & s - N_r \end{vmatrix}}{\begin{vmatrix} s - Y_\beta/u_0 & 1 - Y_r/u_0 \\ -N_\beta & s - N_r \end{vmatrix}} \quad (8.30)$$

$$\frac{\Delta r(s)}{\Delta \delta_r(s)} = \frac{\begin{vmatrix} s - Y_\beta/u_0 & Y_{\delta_r}/u_0 \\ -N_\beta & N_{\delta_r} \end{vmatrix}}{\begin{vmatrix} s - Y_\beta/u_0 & 1 - Y_r/u_0 \\ -N_\beta & s - N_r \end{vmatrix}} \quad (8.31)$$

$$\frac{\Delta \beta(s)}{\Delta \delta_a(s)} = \frac{N_{\delta_r}^\beta(s)}{\Delta_{DR}(s)} = \frac{A_\beta s + B_\beta}{As^2 + Bs + C} \quad (8.32)$$

$$\frac{\Delta r(s)}{\Delta \delta_a(s)} = \frac{N_{\delta_r}^r(s)}{\Delta_{DR}(s)} = \frac{A_r s + B_r}{As^2 + Bs + C} \quad (8.33)$$

In a similar manner the aileron transfer function can be shown to be

$$\frac{\Delta \beta(s)}{\Delta \delta_a(s)} = \frac{N_{\delta_a}^\beta(s)}{\Delta_{DR}(s)} = \frac{A_\beta s + B_\beta}{As^2 + Bs + C} \quad (8.34)$$

$$\frac{\Delta r(s)}{\Delta \delta_a(s)} = \frac{N_{\delta_a}^r(s)}{\Delta_{DR}(s)} = \frac{A_r s + B_r}{As^2 + Bs + C} \quad (8.35)$$

TABLE 8.4
Dutch roll transfer function approximations

A, B_β , or A_r	B, B_β , or B_r	C
$\Delta_{DR}(s)$	1	$-(Y_\beta + u_0 N_r)/u_0$
		$(Y_\beta N_r - N_\beta Y_r + N_\beta u_0)/u_0$
$N_{\delta_r}^B(s)$	Y_r/u_0	$(Y_r N_{\delta_r} - Y_{\delta_r} N_r - N_{\delta_r} u_0)/u_0$
$N_{\delta_r}^r(s)$	N_{δ_r}	$(N_\beta Y_{\delta_r} - Y_\beta N_{\delta_r})/u_0$
$N_{\delta_a}^B(s)$	0	$(Y_r N_{\delta_a} - u_0 N_{\delta_a})/u_0$
$N_{\delta_a}^r(s)$	N_{δ_a}	$-Y_\beta N_{\delta_a}/u_0$

The coefficients of the polynomials in the Dutch roll transfer functions are included in Table 8.4. The denominator coefficients are in the first row and the numerator coefficients are defined for each transfer function in the subsequent rows.

In the previous section, transfer functions were derived for both longitudinal and lateral dynamics based on the approximations to these motions. For a preliminary autopilot design these approximations are appropriate. However, as the autopilot concept is refined and developed it is necessary to examine the autopilot performance using transfer functions based on the complete set of either the longitudinal or lateral equations. This is particularly important for the lateral equations. As we showed in Chapter 5 the lateral approximations do not generally give a very accurate representation of the Dutch roll motion.

The longitudinal and lateral transfer functions for the complete set of equations are determined in the same manner as the approximate transfer functions derived here. The transfer functions for the complete set of rigid body equations are given in Tables 8.5 and 8.6.

8.3 CONTROL SURFACE ACTUATOR

In addition to the various transfer functions that represent the aircraft dynamics, we need to develop the transfer functions for the other elements that make up the control system. This would include the servo actuators to deflect the aerodynamic control surfaces as well as the transfer function for any sensors in the control loop; for example, an attitude gyro, rate gyro, altimeter, or velocity sensor. The transfer functions for most sensors can be approximated by a gain, k . In this section we develop an expression for the transfer function of a simple position control servo that is used to accurately deflect the aerodynamic control surfaces in an automatic system.

Control surface servo actuators can be either electrical, hydraulic, pneumatic, or some combination of the three. The transfer function is similar for each type. We will develop the control surface servo actuator transfer function for a servo based on an electric motor.

TABLE 8.5
Longitudinal control transfer functions

	A	B	C	D	E
Δ_{long}	1	$-M_q - u_0 M_w - Z_w - X_u$	$Z_w M_q - u_0 M_w - X_w Z_u$ $+ X_u (M_q + u_0 M_w + Z_w)$	$-X_u (Z_w M_q - u_0 M_w)$ $+ Z_u (X_w M_q + g M_w)$ $- M_u (u_0 X_w - g)$	
N_δ^{θ}	$M_\delta + Z_\delta M_w$	$X_\delta (Z_u M_w + M_w)$ $+ Z_\delta (M_w - X_u M_w)$ $- M_\delta (X_u + Z_w)$	$X_\delta (Z_u M_w - Z_w M_w)$ $+ Z_\delta (M_u X_w - M_w X_u)$ $+ M_\delta (Z_w X_u - X_w Z_u)$		
N_δ^w	Z_δ	$X_\delta Z_u - Z_\delta (X_u + M_q) + M_\delta u_0$	$X_\delta (u_0 M_u - Z_u M_q)$ $+ Z_\delta X_u M_q - u_0 M_w$	$g(Z_\delta M_u - M_\delta Z_u)$	
N_δ^u	X_δ	$-X_\delta (Z_w + M_q + u_0 M_w) + Z_\delta X_w$	$X_\delta (Z_w M_q - u_0 M_w)$ $- Z_\delta X_w M_q + g M_w$ $+ M_\delta (u_0 X_w - g)$	$g(M_\delta Z_w - Z_\delta M_w)$	

TABLE 8.6
Lateral control transfer functions

	A	B	C	D	E
Δ_{at}	$1 - \frac{I_{xz}^2}{I_x I_z}$	$-Y_v \left(1 - \frac{I_{xz}^2}{I_x I_z} \right) - L_p - N_r$ $- \frac{I_{xz} N_p}{I_x} - \frac{I_{xz} L_r}{I_x}$	$u_0 N_v + L_p (Y_v + N_r) + N_p \left(\frac{I_{xz}}{I_x} Y_v - L_r \right)$ $+ Y_v \left(\frac{I_{xz}}{I_x} L_p + N_r \right) + \frac{I_{xz}}{I_x} L_v$	$-u_0 N_v L_p - Y_v (N_p L_r - L_p N_r)$ $+ u_0 N_p L_v - g \left(L_v + \frac{I_{xz}}{I_x} N_v \right)$	$g(L_v N_r - N_v L_r)$
N_s^v	$Y_s \left(1 - \frac{I_{xz}^2}{I_x I_z} \right)$	$-Y_s \left(L_p + N_r + \frac{I_{xz}}{I_x} N_p + \frac{I_{xz}}{I_z} L_r \right)$ $- u_0 \left(\frac{I_{xz}}{I_z} L_s + N_s \right)$	$Y_s (L_p N_r - N_p L_r) + u_0 (N_s L_p - L_s N_p)$ $+ g \left(L_s + \frac{I_{xz}}{I_x} N_s \right)$	$g(N_s L_r - L_s N_p)$	
N_s^ϕ	$L_s + \frac{I_{xz}}{I_x} N_s$	$Y_s \left(L_v + \frac{I_{xz}}{I_x} N_v \right) - L_s (N_r + Y_v)$ $+ N_s \left(L_r - \frac{I_{xz}}{I_x} Y_v \right)$	$Y_s (L_r N_v - L_v N_r) + L_s (Y_v N_r + u_0 N_v)$ $- N_s (u_0 L_v + Y_v L_r)$		
N_s^r	$N_s + \frac{I_{xz}}{I_z} L_s$	$Y_s \left(N_v + \frac{I_{xz}}{I_x} L_v \right)$ $+ L_s \left(N_p - \frac{I_{xz}}{I_z} Y_c \right)$ $- N_s (Y_v + L_p)$	$Y_s (L_v N_p - N_v L_p) - L_s Y_v N_p + N_s Y_v L_p$	$g(L_s N_v - N_s L_v)$	

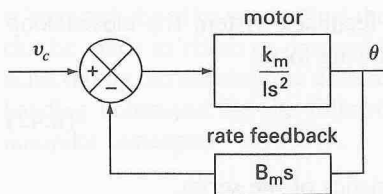


FIGURE 8.2
Motor with rate feedback.

The torque produced by an electric motor is proportional to the control voltage as follows:

$$T_m = k_m v_c \quad (8.36)$$

where k_m is a constant. The angular position of the motor shaft can be determined from the equation

$$I \ddot{\theta} = T_m \quad (8.37)$$

The relationship between the angular position of the motion shaft (output) and the motor control voltage (input) is given by the transfer function

$$\frac{\theta}{v_c} = \frac{k_m}{Is^2} \quad (8.38)$$

In general, the motor will incorporate a rate feedback loop as illustrated in Figure 8.2. The transfer function for the system with rate feedback can be shown to be

$$\frac{\theta}{v_c} = \frac{k}{s(\tau_m s + 1)} \quad (8.39)$$

where $\tau_m = \frac{I}{k_m B_m}$ and $k = \frac{1}{B_m}$ (8.40)

The motor time constant τ_m is a measure of how fast the motor responds to a change in control voltage. If τ_m is small, the motor responds rapidly and the transfer function of the motor with rate feedback can be approximated as

$$\frac{\theta}{v_c} = \frac{k}{s} \quad (8.41)$$

A simple position control servo system can be developed from the control diagram shown in Figure 8.3. The motor shaft angle, θ , can be replaced by the flap angle,

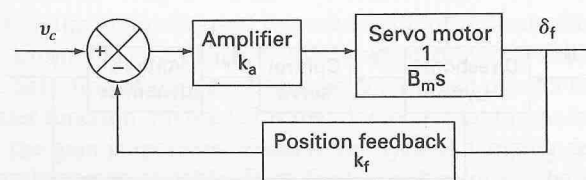


FIGURE 8.3
Simple position control servo for control surface deflection.

δ_f , of the control surface. For the positional feedback system the closed loop transfer function can be shown to have the following form:

$$\frac{\delta_f}{v_c} = \frac{k}{\tau s + 1} \quad (8.42)$$

where k and τ are defined in terms of characteristics of the servo,

$$k = 1/k_f \quad \text{and} \quad \tau = \frac{B_m}{k_f k_a} \quad (8.43)$$

The time constant of the control surface servo is typical of the order of 0.1 s. In the problems that follow we assume this value as representative of typical control surface servo time constants.

8.4 DISPLACEMENT AUTOPILOT

One of the earliest autopilots to be used for aircraft control is the so-called displacement autopilot. A displacement type autopilot can be used to control the angular orientation of the airplane. Conceptually, the displacement autopilot works in the following manner. In a pitch attitude displacement autopilot, the pitch angle is sensed by a vertical gyro and compared with the desired pitch angle to create an error angle. The difference or error in pitch attitude is used to produce proportional displacements of the elevator so that the error signal is reduced. Figure 8.4 is a block diagram of either a pitch or roll angle displacement autopilot.

The heading angle of the airplane also can be controlled using a similar scheme. The heading angle is sensed by a directional gyro and the error signal is used to displace the rudder to reduce the error signal. A displacement heading autopilot also is shown in Figure 8.5.

In practice, the displacement autopilot is engaged once the airplane has been trimmed in straight and level flight. To maneuver the airplane while the autopilot

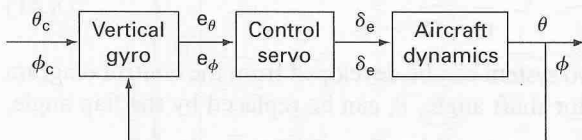


FIGURE 8.4
A roll or pitch displacement autopilot.

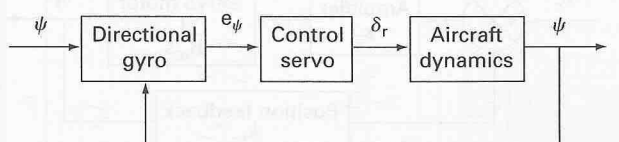


FIGURE 8.5
A heading displacement autopilot.

is engaged, the pilot must adjust the commanded signals. For example, the airplane can be made to climb or descend by changing the pitch command. Turns can be achieved by introducing the desired bank angle while simultaneously changing the heading command. In the following sections we examine several displacement autopilot concepts.

8.4.1 Pitch Displacement Autopilot

The basic components of a pitch attitude control system are shown in Figure 8.4. For this design the reference pitch angle is compared with the actual angle measured by a gyro to produce an error signal to activate the control servo. In general the error signal is amplified and sent to the control surface actuator to deflect the control surface. Movement of the control surface causes the aircraft to achieve a new pitch orientation, which is fed back to close the loop.

To illustrate how such an autopilot would be designed, we will examine this particular pitch displacement autopilot concept for a business jet aircraft. Once we have decided on a control concept, our next step must be to evaluate the performance of the control system. To accomplish this we must define the transfer functions for each of the elements in the block diagram describing the system. For this discussion we assume that the transfer functions of both the gyro and amplifier can be represented by simple gains. The elevator servo transfer function can be represented as a first-order system:

$$\frac{\delta_e}{v} = \frac{k_a}{\tau s + 1}$$

where δ_e , v , k_a , and τ are the elevator deflection angle, input voltage, elevator servo gain, and servomotor time constant. Time constants for typical servomotors fall in a range 0.05–0.25 s. For our discussion we assume a time constant of 0.1 s. Finally, we need to specify the transfer function for the airplane. The transfer function relating the pitch attitude to elevator deflection was developed earlier. To keep the description of this design as simple as possible, we represent the aircraft dynamics by using the short-period approximation. The short-period transfer function for the business jet in Appendix B can be shown to be

$$\frac{\Delta\theta}{\Delta\delta_e} = \frac{-2.0(s + 0.3)}{s(s^2 + 0.65s + 2.15)}$$

Figure 8.6 is the block diagram representation of the autopilot. The problem now is one of determining the gain k_a so that the control system will have the desired performance. Selection of the gain k_a can be determined using a root locus plot of the loop transfer function. Figure 8.7 is the root locus plot for the business jet pitch autopilot. As the gain is increased from 0, the system damping decreases rapidly and the system becomes unstable. Even for low values of k_a , the system damping would be too low for satisfactory dynamic performance. The reason for the poor performance of this design is that the airplane has very little natural damping. To

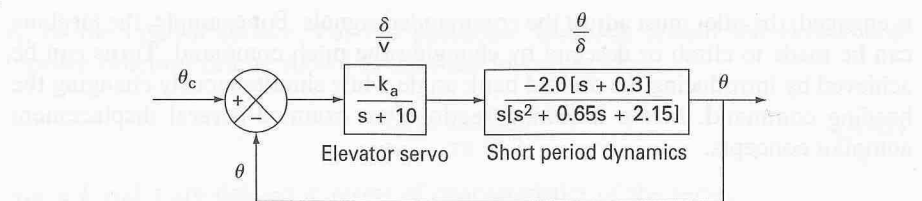


FIGURE 8.6

A pitch displacement autopilot for a business jet.

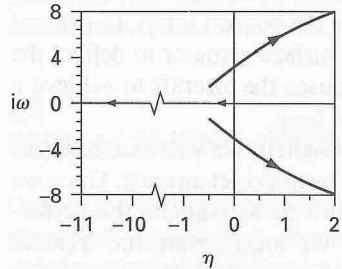


FIGURE 8.7

Root locus plot of the system gain for a pitch displacement autopilot.

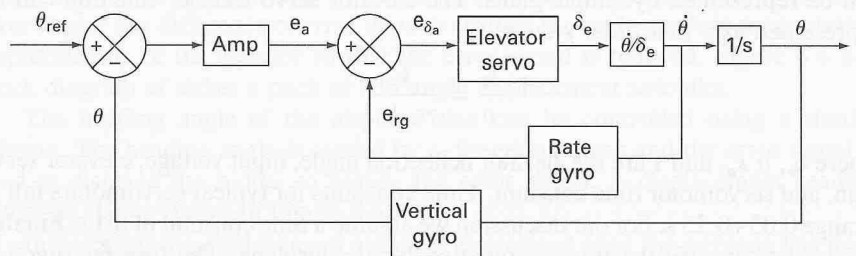


FIGURE 8.8

A pitch attitude control system employing pitch rate feedback.

improve the design we could increase the damping of the short-period mode by adding an inner feedback loop. Figure 8.8 is a block diagram of a displacement autopilot with pitch rate feedback for improved damping. In the inner loop the pitch rate is measured by a rate gyro and fed back to be added with the error signal generated by the difference in pitch attitude. Figure 8.9 is a block diagram for the business jet when pitch rate is incorporated into the design. For this problem we now have two parameters to select; namely, the gains k_a and k_{rg} . The root locus method can be used to pick both parameters. The procedure essentially is by trial and error. First, the root locus diagram is determined for the inner loop, a gyro gain is selected, and then the outer root locus plot is constructed. Several iterations may be required until the desired overall system performance is achieved.

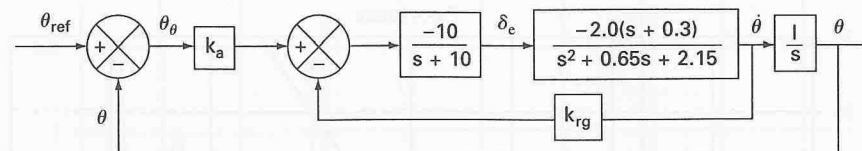


FIGURE 8.9

A business jet pitch attitude control system with pitch rate feedback.

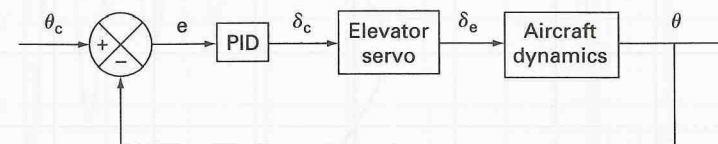


FIGURE 8.10

Pitch attitude autopilot with a PID controller.

EXAMPLE PROBLEM 8.1. Use the PID controller for a pitch attitude autopilot as illustrated in Figure 8.10. The transfer functions for each component are given in Table 8.7.

Solution. Using the Ziegler and Nichols method discussed in Section 7.8, the PID gains can be estimated from the ultimate gain k_{pu} , which is the gain for which the system is marginally stable when only the proportional control is being used. Figure 8.11 is the root locus sketch of the transfer function:

$$G(s)H(s) = \frac{3.0k_p}{(s + 10)(s^2 + 2s + 5)}$$

The root locus crosses the imaginary axis at $s = \pm 5.13i$. The gain of the system can be found from the magnitude criteria to be $k_{pu} = 88.7$. The period, $T_u = 2\pi/\omega = 1.22$. Table 8.8 gives the gains for the proportional, proportional-integral and proportional-integral-derivative controllers. Figure 8.12 shows the response of the pitch attitude

TABLE 8.7
Data for Example Problem 8.1

Control element	Parameters	Transfer function
PID	$k_p = ?$ $k_i = ?$ $k_d = ?$	$\delta_c = k_p + \frac{k_i}{s} + k_d s$
Elevator servo	$A = -0.1$ $\tau = 0.1$	$\frac{\delta_e}{\delta_c} = \frac{A}{\tau s + 1}$
Aircraft dynamics	$M_{\delta_e} = -3 \text{ s}^{-2}$ $M_q = -2 \text{ s}^{-1}$ $M_\alpha = -5 \text{ s}^{-2}$	$\frac{\theta}{\delta_e} = \frac{M_{\delta_e}}{s^2 - M_q s - M_\alpha}$

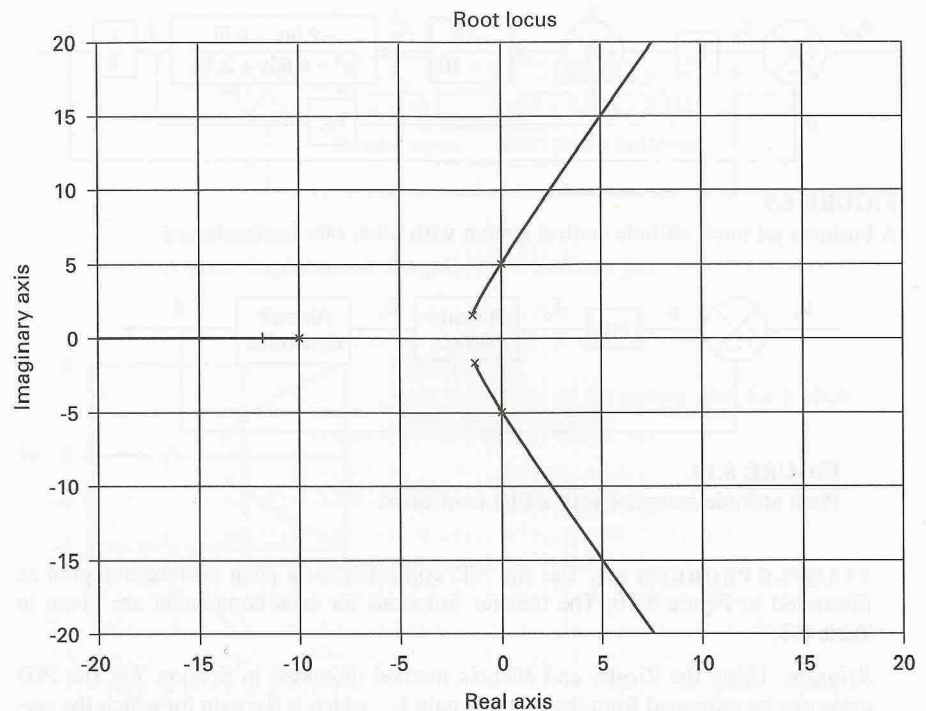


FIGURE 8.11
Root locus plot of $G(s)H(s)$.

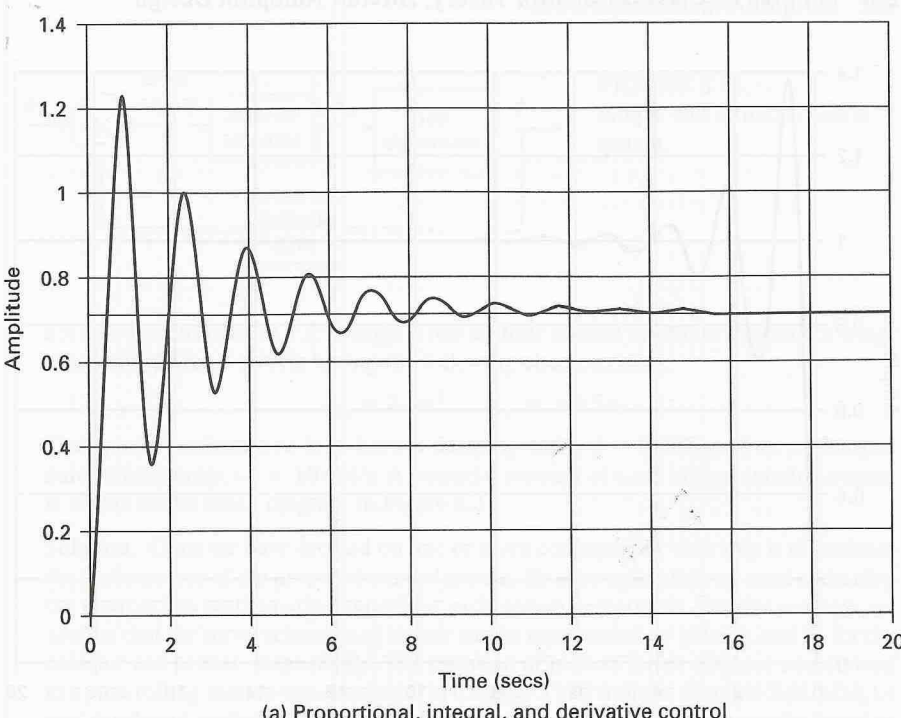
TABLE 8.8
Gains for P, PI, and PID controllers

P control	$k_p = 0.5k_{pu} = 44.35$
PI control	$k_p = 0.45k_{pu} = 39.92$ $k_i = 0.45k_{pu}/(0.83T_u) = 39.42$
PID control	$k_p = 0.6k_{pu} = 53.22$ $k_i = 0.6k_{pu}/(0.5T_u) = 87.24$ $k_d = 0.6k_{pu}(0.125T_u) = 8.12$

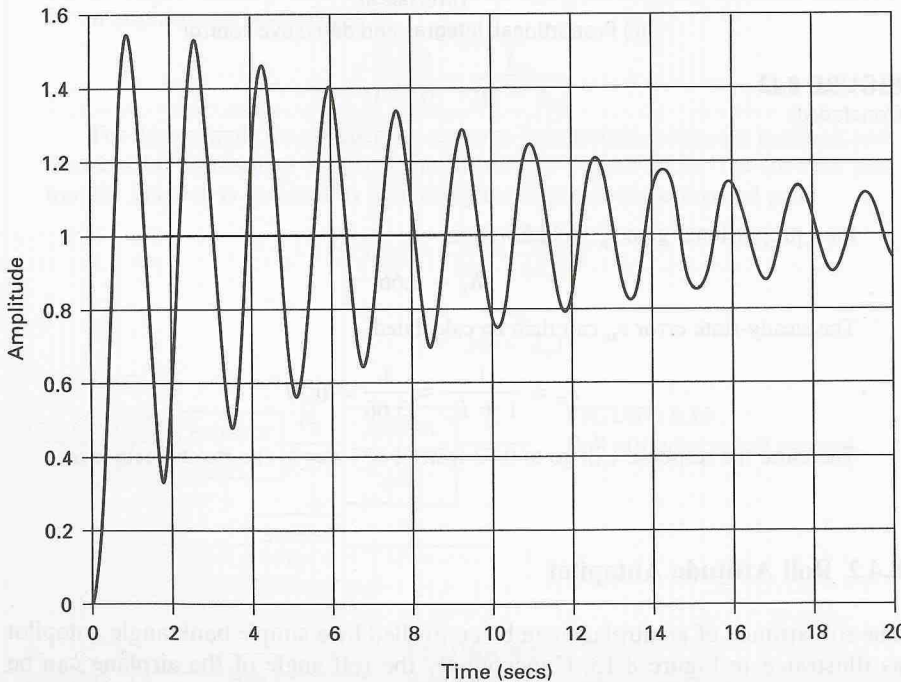
autopilot for the three different controllers to a step input. Notice that the proportional controller has a steady-state error; that is, it does not go to 1 but converges to a value of approximately 0.7. The magnitude of the steady-state error can be predicted using the steady-state error constants in Chapter 7:

$$e_{ss} = \frac{1}{1 + K_p}$$

where $K_p = \lim_{s \rightarrow 0} G(s)H(s) = \lim_{s \rightarrow 0} \frac{3.0k_p}{s^3 + 12s^2 + 25s + 50}$

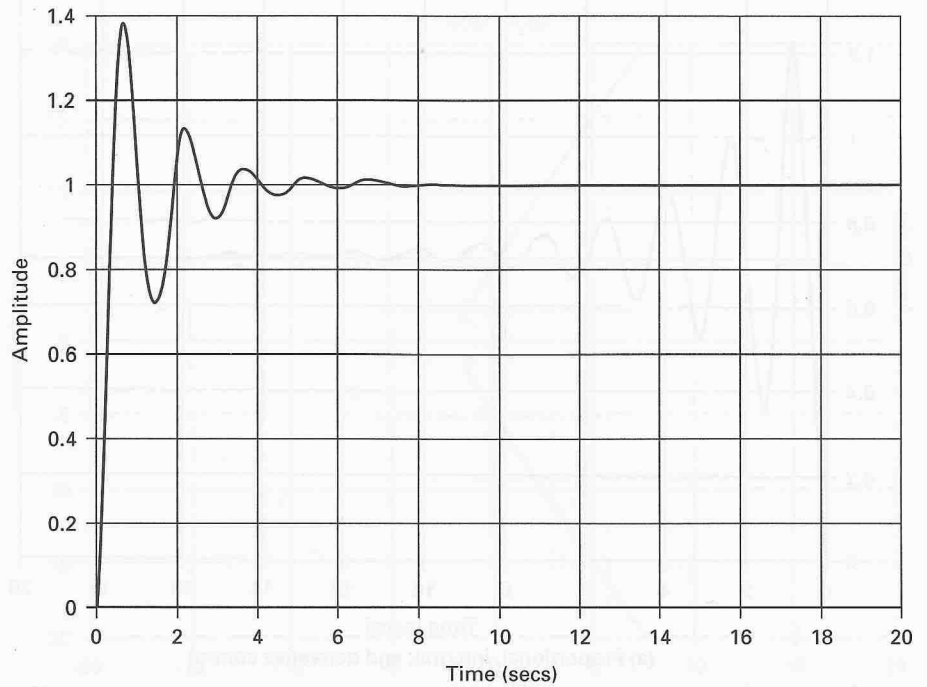


(a) Proportional, integral, and derivative control



(b) Proportional plus integral control

FIGURE 8.12
Response to a step input of a pitch autopilot with either a P, PI, or PID controller.



(c) Proportional, integral, and derivative control

FIGURE 8.12
Concluded.

for a proportional gain $k_p = 44.35$

$$K_p = 2.66$$

The steady-state error e_{ss} can then be calculated:

$$e_{ss} = \frac{1}{1 + K_p} = \frac{1}{3.66} = 0.27$$

Therefore the response will go to 0.73 instead of 1 due to the steady-state error.

8.4.2 Roll Attitude Autopilot

The roll attitude of an airplane can be controlled by a simple bank angle autopilot as illustrated in Figure 8.13. Conceptually the roll angle of the airplane can be maintained at whatever angle one desires. In practice we would typically design the autopilot to maintain a wings level attitude or $\phi = 0$. The autopilot is composed of a comparator, aileron actuator, aircraft equation of motion (i.e., transfer function), and an attitude gyro to measure the airplane's roll angle.

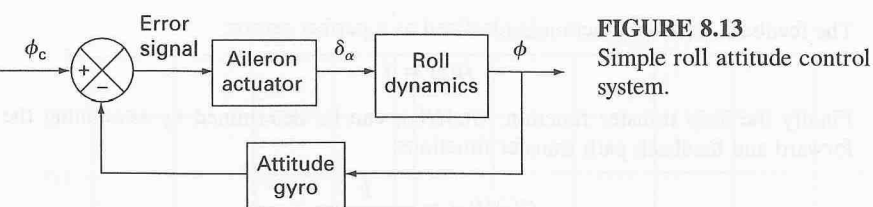


FIGURE 8.13
Simple roll attitude control system.

EXAMPLE PROBLEM 8.2. Design a roll attitude control system to maintain a wings level attitude for a vehicle having the following characteristics:

$$L_{\delta_a} = 2.0/s^2 \quad L_p = -0.5/s$$

The system performance is to have a damping ratio, $\zeta = 0.707$, and an undamped natural frequency, $\omega_n = 10 \text{ rad/s}$. A potential concept of a roll attitude control system is shown in the block diagram in Figure 8.14.

Solution. Once we have decided on one or more concepts our next step is to evaluate the performance of the proposed control system. To accomplish this we need to develop the appropriate mathematical model for each system component. For this example we assume that the servo actuator and sensor can be represented by gains k_a and k_s , for the actuator and sensor, respectively. The equation of motion for an airplane constrained to a pure rolling motion was developed in Chapter 5 and transfer function $\Delta\phi(s)/\Delta\delta_a(s)$ was developed earlier in this chapter. The roll angle to aileron input transfer function for an airplane can be shown to be

$$\frac{\Delta\phi(s)}{\Delta\delta_a(s)} = \frac{L_{\delta_a}}{s(s - L_p)}$$

For this example we consider the sensor to be a perfect device; the feedback path then can be represented as a unity feedback (see Figure 8.15). The forward path transfer function is obtained by combining the elements in the forward path:

$$\begin{aligned} G(s) &= \frac{\Delta\delta_a(s)}{e(s)} \frac{\Delta\phi(s)}{\Delta\delta_a(s)} \\ &= k_a \frac{L_{\delta_a}}{s(s - L_p)} \end{aligned}$$

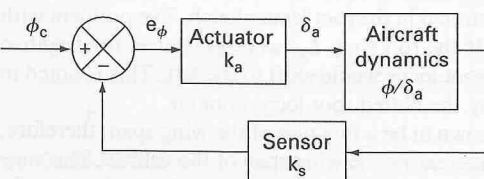


FIGURE 8.14
Roll attitude control concept.

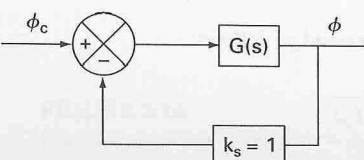


FIGURE 8.15
Simplified roll control system.

The feedback transfer function is idealized as a perfect sensor:

$$H(s) = 1$$

Finally the loop transfer function, $G(s)H(s)$, can be determined by combining the forward and feedback path transfer functions:

$$G(s)H(s) = \frac{k}{s(s - L_p)}$$

where

$$k = k_a L_{\delta_a}$$

$$G(s)H(s) = \frac{k}{s(s + 0.5)}$$

The desired damping ratio of $\zeta = 0.707$ can be achieved with the present control system. The gain for the system is determined by drawing a line from the origin at 45° as indicated in the root locus plot. Recall that the damping ratio was shown to be equal to the following expression:

$$\zeta = \cos \theta$$

where θ is measured from the positive real axis in the counterclockwise direction. Any root intersecting this line has a damping ratio of 0.707. The gain at this point can be determined from the magnitude criteria as follows:

$$\frac{|k|}{|s| |s + 0.5|} = 1$$

where $s = -0.25 + 0.25i$.

Substituting s into the magnitude equation and determining the magnitude of each component yields a value for k :

$$k = 0.0139$$

For this example we see that it is possible to select a gain so that the damping ratio requirement is satisfied; however, the undamped natural frequency is much lower than specified:

$$\omega_n = 0.35 \text{ rad/s}$$

Recall that the undamped natural frequency is equal to the radial distance from the origin to the point on the locus as illustrated in the root locus sketch. The problem with this system is the low roll damping. If the roll root, L_p , were greater in the negative sense, the vertical asymptotes of the root locus would shift to the left. This is noted in the root locus sketch (Figure 8.16) by the dotted root locus contour.

L_p , the roll damping root, was shown to be a function of the wing span; therefore, we could make L_p more negative by increasing the wing span of the vehicle. This may be impractical and so we need to look at providing increased damping by means of a stability augmentation system. This can be accomplished by incorporating a rate feedback loop as illustrated in Figure 8.17.

The inner loop transfer function can be expressed as follows:

$$\frac{\Delta p(s)}{\Delta \delta_a(s)} = \frac{L_{\delta_a}}{(s - L_p)}$$

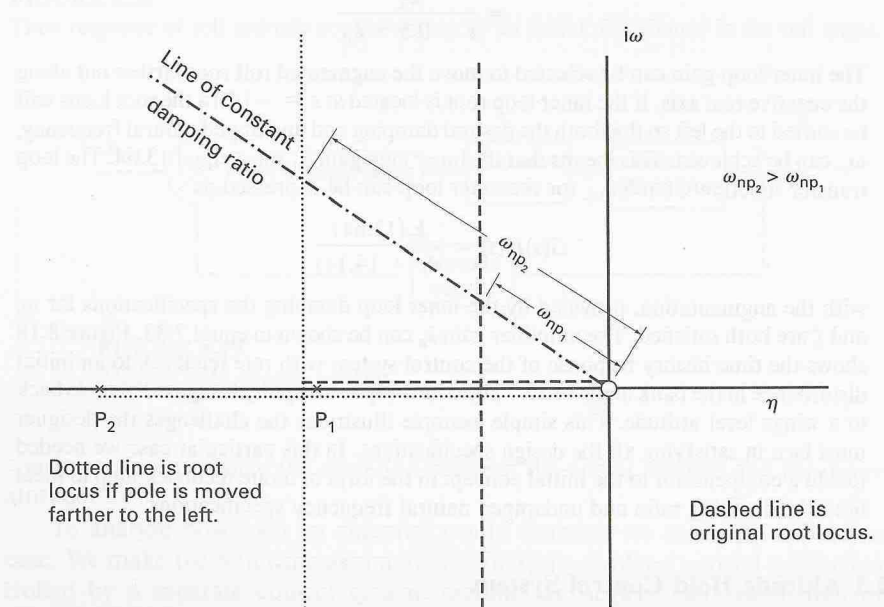
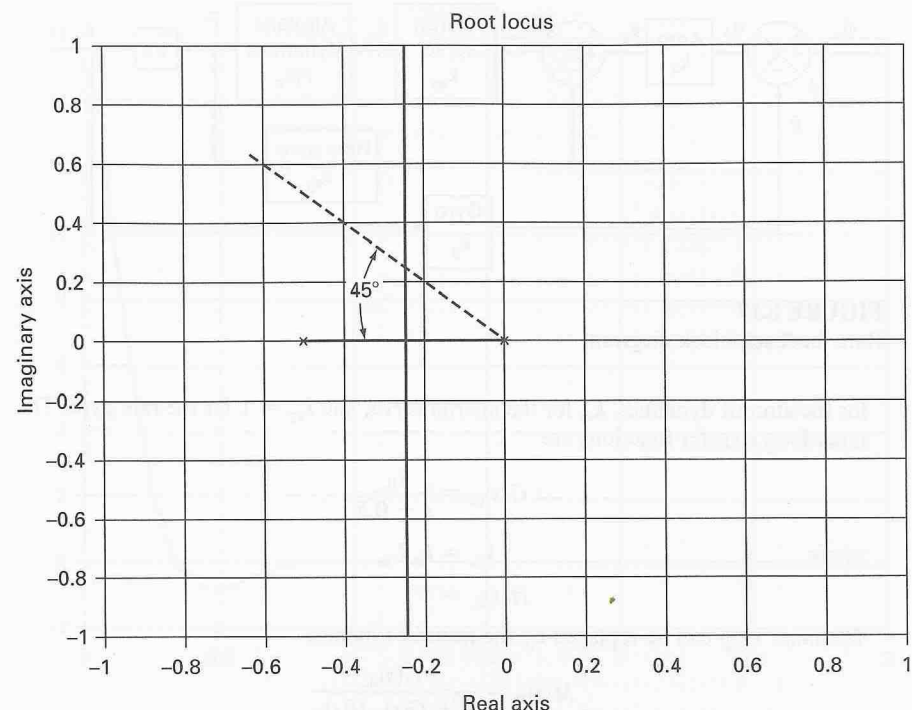
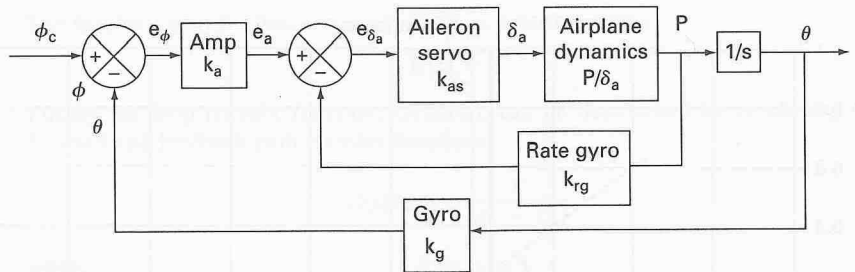


FIGURE 8.16
Root locus plot of $G(s)H(s) = k/s(s + 0.5)$.

**FIGURE 8.17**

Rate feedback block diagram.

for the aircraft dynamics, k_{as} for the aileron servo, and $k_{rg} = 1$ for the rate gyro. The inner loop transfer functions are

$$G(s)_{IL} = \frac{k_{IL}}{s + 0.5}$$

where

$$k_{IL} = k_{as}L_{\delta_a}$$

$$H(s)_{IL} = 1$$

The inner loop can be replaced by the transfer function

$$\begin{aligned} M(s)_{IL} &= \frac{G(s)_{IL}}{1 + G(s)_{IL}H(s)_{IL}} \\ &= \frac{k_{IL}}{s + 0.5 + k_{IL}} \end{aligned}$$

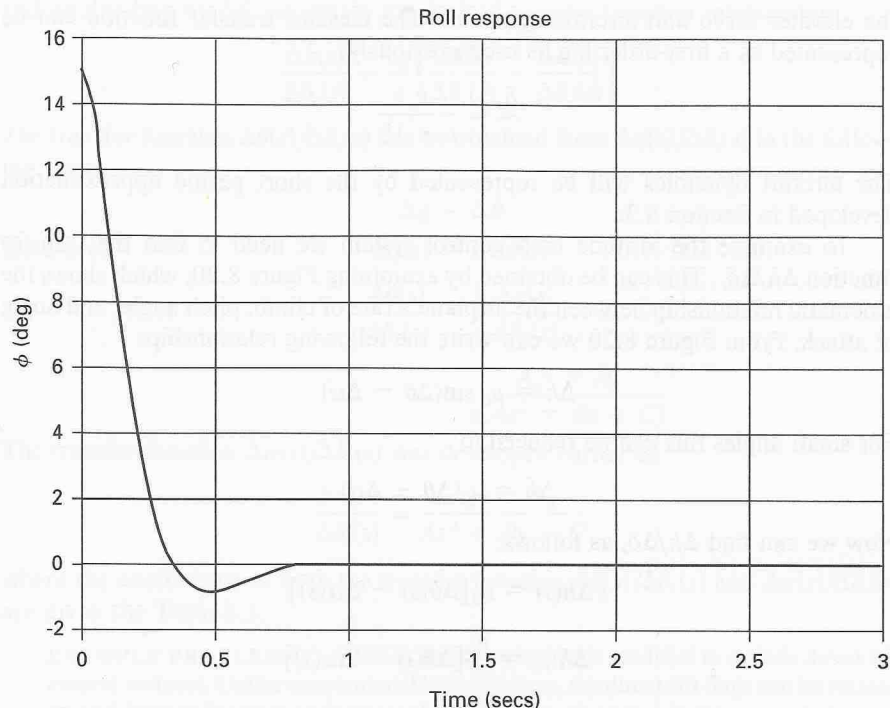
The inner loop gain can be selected to move the augmented roll root farther out along the negative real axis. If the inner loop root is located at $s = -14.14$ the root locus will be shifted to the left so that both the desired damping and undamped natural frequency, ω_n , can be achieved. This means that the inner loop gain k_{IL} must equal 13.64. The loop transfer function $G(s)H(s)_{OL}$ for the outer loop can be expressed as

$$G(s)H(s) = \frac{k_a(13.64)}{s(s + 14.14)}$$

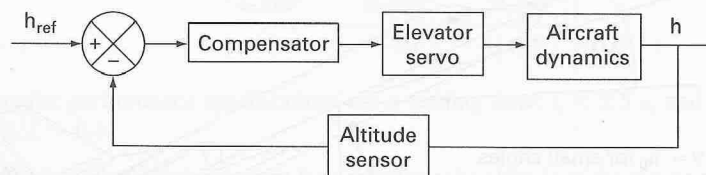
with the augmentation, provided by the inner loop damping the specifications for ω_n and ζ are both satisfied. The amplifier gain k_a can be shown to equal 7.33. Figure 8.18 shows the time history response of the control system with rate feedback to an initial disturbance in the bank angle of 15° . The control system rapidly brings the vehicle back to a wings level attitude. This simple example illustrates the challenges the designer must face in satisfying all the design specifications. In this particular case we needed to add a compensator to the initial concept in the form of a rate feedback loop to meet both the damping ratio and undamped natural frequency specifications.

8.4.3 Altitude Hold Control System

The altitude of an airplane can be maintained by an altitude hold autopilot. A simplified altitude hold autopilot is shown in Figure 8.19. Basically the autopilot is

**FIGURE 8.18**

Time response of roll attitude control system to an initial disturbance in the roll angle.

**FIGURE 8.19**

Altitude hold control system.

constructed to minimize the deviation between the actual altitude and the desired altitude.

To analyze how such an autopilot would function we examine an idealized case. We make the following assumptions: First, the airplane's speed will be controlled by a separate control system; second, we neglect any lateral dynamic effects. With these restrictions we are assuming that the only motion possible is in the vertical plane. The transfer functions necessary for performing this analysis are

the elevator servo and aircraft dynamics. The elevator transfer function can be represented as a first-order lag as used previously:

$$\frac{\delta_e}{e} = \frac{k_a}{s + 10}$$

The aircraft dynamics will be represented by the short period approximation developed in Section 8.3.

To examine the altitude hold control system we need to find the transfer function $\Delta h/\Delta\delta_e$. This can be obtained by examining Figure 8.20, which shows the kinematic relationship between the airplane's rate of climb, pitch angle, and angle of attack. From Figure 8.20 we can write the following relationship:

$$\Delta h = u_0 \sin(\Delta\theta - \Delta\alpha)$$

For small angles this can be reduced to

$$\Delta h = u_0(\Delta\theta - \Delta\alpha)$$

Now we can find $\Delta h/\Delta\delta_e$ as follows:

$$s\Delta h(s) = u_0[\Delta\theta(s) - \Delta\alpha(s)]$$

or

$$\Delta h(s) = \frac{u_0}{s}[\Delta\theta(s) - \Delta\alpha(s)]$$

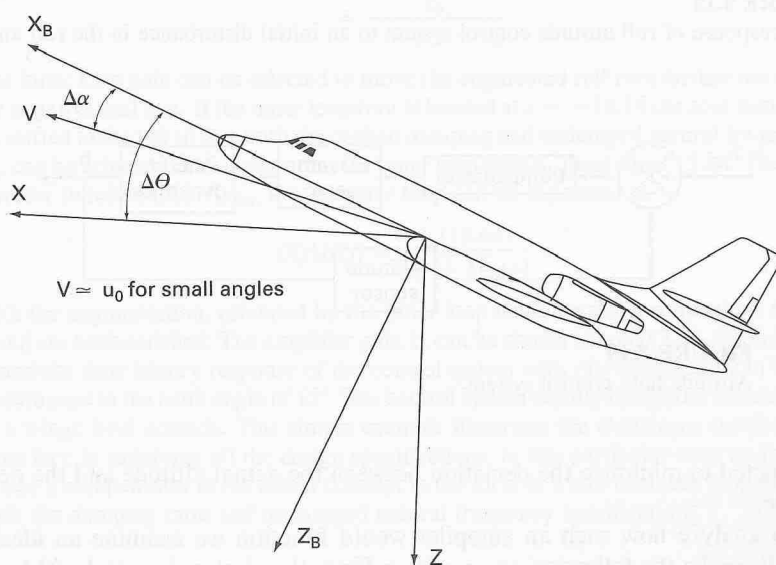


FIGURE 8.20

Kinematic relationship for determining vertical rate of climb.

and on dividing by $\Delta\delta_e$ we obtain the desired transfer function relationship:

$$\frac{\Delta h(s)}{\Delta\delta_e(s)} = \frac{u_0}{s} \left[\frac{\Delta\theta(s)}{\Delta\delta_e(s)} - \frac{\Delta\alpha(s)}{\Delta\delta_e(s)} \right]$$

The transfer function $\Delta\theta(s)/\Delta\delta_e(s)$ can be obtained from $\Delta q(s)/\Delta\delta_e(s)$ in the following way:

$$\Delta q = \Delta\dot{\theta}$$

therefore,

$$\Delta q(s) = s \Delta\theta(s)$$

or

$$\frac{\Delta\theta(s)}{\Delta\delta_e(s)} = \frac{1}{s} \frac{\Delta q(s)}{\Delta\delta_e(s)}$$

$$= \frac{A_q s + B_q}{s(A s^2 + B s + C)}$$

The transfer function $\Delta\alpha(s)/\Delta\delta_e(s)$ was developed earlier as

$$\frac{\Delta\alpha(s)}{\Delta\delta_e(s)} = \frac{A_\alpha s + B_\alpha}{A s^2 + B s + C}$$

where the coefficients in both the transfer function $\Delta\theta(s)/\Delta\delta_e(s)$ and $\Delta\alpha(s)/\Delta\delta_e(s)$ are given in Table 8.3.

EXAMPLE PROBLEM 8.3. A STOL transport has been modified to include direct-lift control surfaces. Unlike conventional high-lift flaps, the direct-lift flaps can be rotated up and down to increase or decrease the lift force on the wing. In this example, we are going to design an altitude hold control system that uses the direct-lift control surfaces. To simplify our analysis we assume that the airplane's velocity and pitch attitude are controlled by separate autopilots. The aerodynamic characteristics of the STOL airplane and the desired performance expected of the altitude autopilot follow:

$Z_\alpha \text{ ft/s}^2$	$Z_{\delta_f} \text{ ft/s}^2$	$u_0 \text{ ft/s}$
-560	-50	400

Autopilot performance specifications are a settling time, $t_s < 2.5$ s, and a damping ratio, $\zeta = 0.6$.

Solution. One potential concept for controlling the altitude of the airplane is given in Figure 8.21. The transfer functions for each element of the control system are described next. The amplifier transfer function is a gain, k_a , the direct-lift servo is modeled as a first-order lag, and the altitude sensor is assumed to be a perfect sensor, which gives us a unity feedback system:

$$\frac{e_h}{e_s} = k_a$$

$$\frac{\delta_f}{e_s} = \frac{-10}{s + 10}$$

The transfer function for the aircraft dynamics can be obtained from the equation of motion in the vertical direction. Recall that we have assumed that the speed and pitch

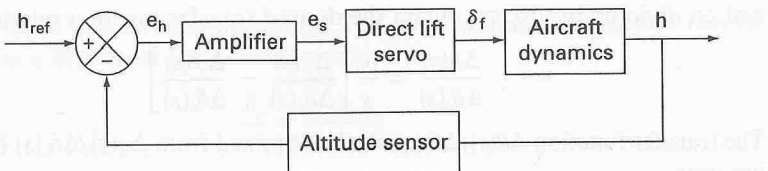


FIGURE 8.21
Altitude control concept.

attitude of the airplane are held at some desired values by separate autopilots. The equation of motion in the vertical direction is given by

$$\sum \text{Forces in vertical direction} = m \frac{dw}{dt}$$

or

$$W + Z = m \frac{dw}{dt}$$

Expressing the variables in terms of a reference value and a perturbation yields

$$W + Z_0 + \Delta Z = m \frac{d}{dt} (w_0 + \Delta w)$$

but $W + Z_0 = 0$ and $w_0 = 0$; for level equilibrium flight therefore,

$$\Delta Z = m \Delta \dot{w}$$

The change in the aerodynamic force ΔZ is assumed to be only a function of Δw and $\Delta \delta_f$, that is,

$$\Delta Z = \frac{\partial Z}{\partial w} \Delta w + \frac{\partial Z}{\partial \delta_f} \Delta \delta_f$$

Substituting into the differential equation yields

$$\Delta \dot{w} = Z_w \Delta w + Z_{\delta_f} \Delta \delta_f$$

where

$$Z_w = \frac{\partial Z / \partial w}{m}, \quad Z_{\delta_f} = \frac{\partial Z / \partial \delta_f}{m}$$

Recall that Z_w and Z_α are related in the following manner:

$$Z_w = \frac{\partial Z / \partial w}{m} = \frac{1}{u_0} \frac{\partial Z / \partial (w/u_0)}{m} = \frac{1}{u_0} Z_\alpha$$

The transfer function $\Delta h / \Delta \delta_f$ now can be obtained:

$$\frac{\Delta w(s)}{\Delta \delta_f(s)} = \frac{Z_{\delta_f}}{s - Z_w}$$

but $\dot{h} = -\Delta w$; therefore,

$$\frac{\Delta h(s)}{\Delta \delta_f(s)} = -\frac{1}{s} \frac{Z_{\delta_f}}{(s - Z_w)}$$

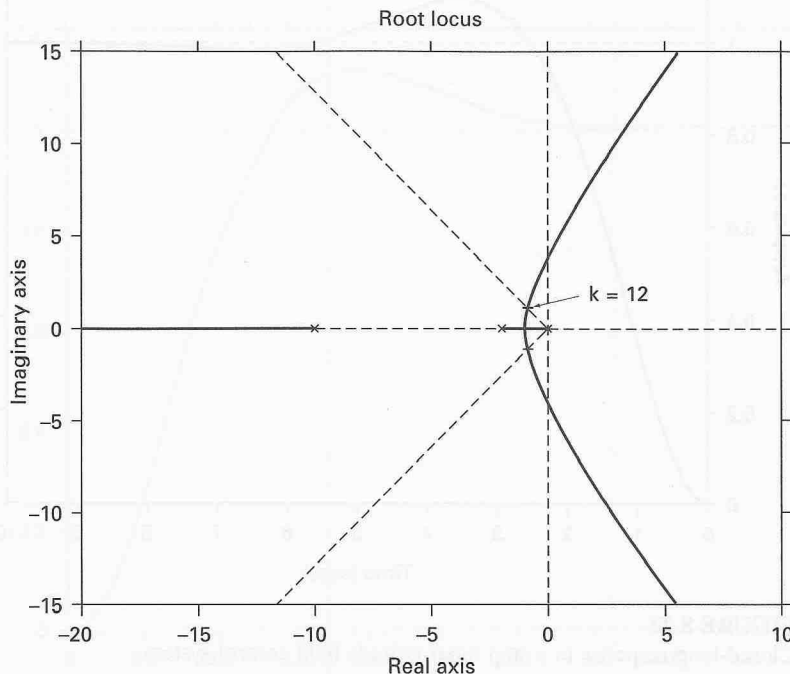


FIGURE 8.22
Root locus plot of $G(s)H(s)$, altitude hold control system.

Substituting the aerodynamic data for the STOL transport yields

$$\frac{\Delta h(s)}{\Delta \delta_f(s)} = -\frac{50}{s(s + 1.4)}$$

The forward path transfer function is

$$G(s) = \frac{k}{s(s + 1.4)(s + 10)}$$

where $k = k_a(-10)(-50) = 500 k_a$.

The root locus plot of $G(s)H(s)$ is shown in Figure 8.22. Although the desired damping ratio $\zeta = 0.6$ can be achieved, the settling time is greater than 2.5 s. The closed-loop system response to a unit step change in altitude is shown in Figure 8.23. To improve the system performance we need to include some form of compensation. A lead circuit in the forward path can be used to improve the system performance. Figure 8.24 shows the root locus plot of $G(s)H(s)$ with the addition of a lead circuit

$$\text{T.F.} = \frac{s + a}{s + b} \quad a < b$$

The zero of the lead circuit was positioned just to the left of the pole at $s = -1.4$. With the addition of the lead circuit the root locus plot is shifted to the left compared to the uncompensated system. For the compensated system we can meet both the damping ratio and settling time specification (Figure 8.25).

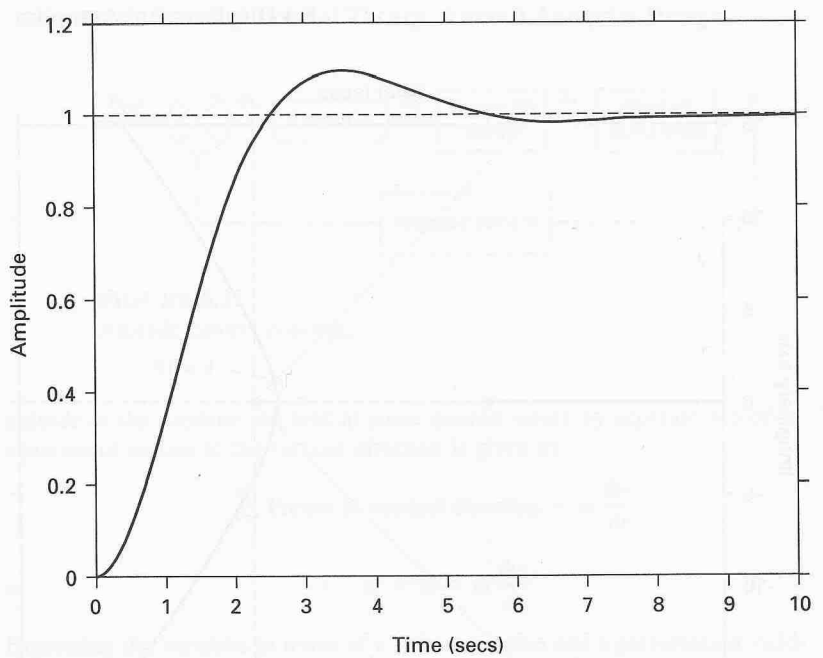


FIGURE 8.23
Closed-loop response to a step input altitude hold control system.

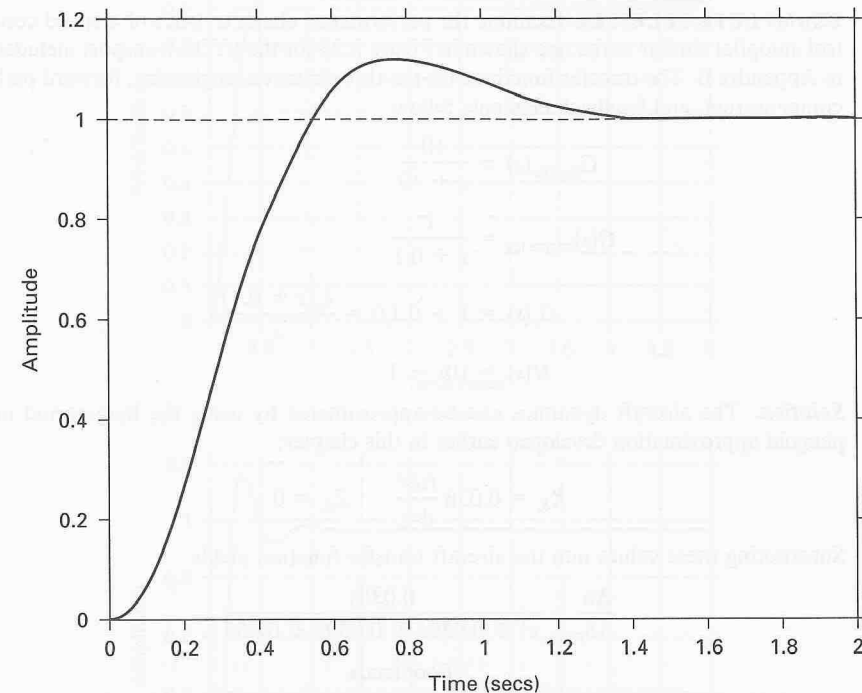


FIGURE 8.25
Closed-loop response to a step input for an altitude hold control system with a compensator.

8.4.4 Velocity Hold Control System

The forward speed of an airplane can be controlled by changing the thrust produced by the propulsion system. The function of the speed control system is to maintain some desired flight speed. This is accomplished by changing the engine throttle setting to increase or decrease the engine thrust. Figure 8.26 is a simplified concept for a speed control system described in [8.3]. The components that make up the system include a compensator, engine throttle, aircraft dynamics, and a feedback path consisting of the velocity and acceleration feedback.

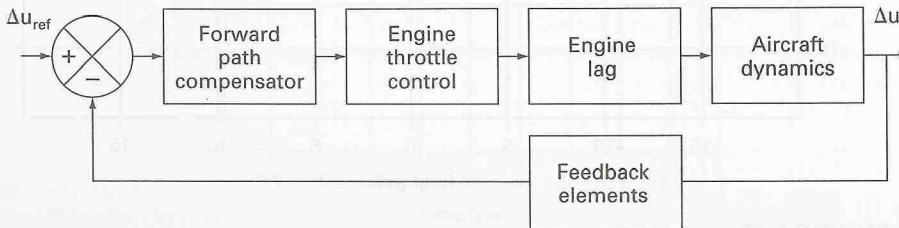


FIGURE 8.26
A block diagram for a speed control system.

EXAMPLE PROBLEM 8.4. Examine the performance characteristics of a speed control autopilot similar to the one shown in Figure 8.26 for the STOL transport included in Appendix B. The transfer functions for the throttle servo, engine lag, forward path compensation, and feedback elements follow:

$$G_{\text{throttle}}(s) = \frac{10}{s + 10}$$

$$G(s)_{\text{engine lag}} = \frac{1}{s + 0.1}$$

$$G_c(s) = 1 + 0.1/s = \frac{k_a(s + 0.1)}{s}$$

$$H(s) = 10s + 1$$

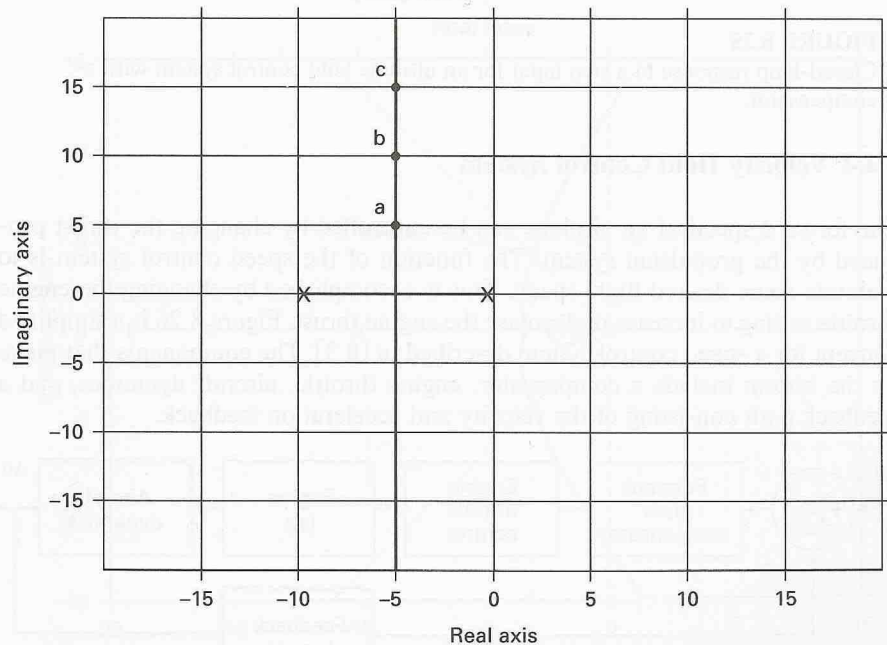
Solution. The aircraft dynamics can be approximated by using the long-period or phugoid approximation developed earlier in this chapter:

$$X_{\delta_T} = 0.038 \frac{\text{ft/s}^2}{\text{deg}} \quad Z_{\delta_T} = 0$$

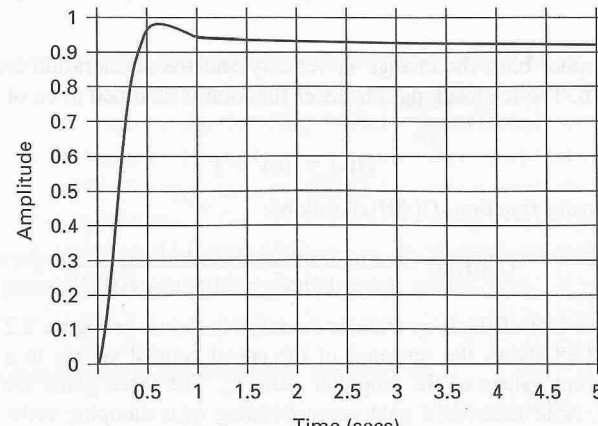
Substituting these values into the aircraft transfer function yields

$$\frac{\Delta u}{\Delta \delta_T} = \frac{0.038s}{s^2 + 0.039s + 0.039s + 0.053}$$

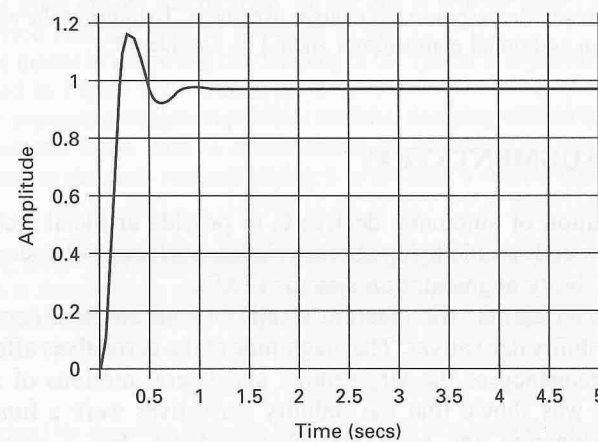
Root locus

**FIGURE 8.27**

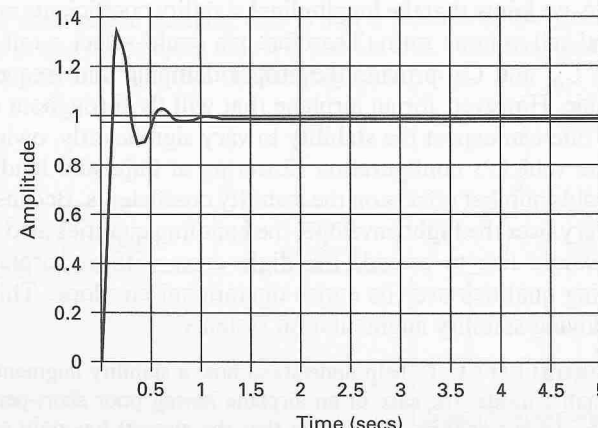
$$\text{Root locus plot } G(s)H(s) = \frac{3.8k_a(s + 0.1)}{(s + 10)(s^2 + 0.039s + 0.053)}.$$



(a) Gain a



(b) Gain b



(c) Gain c

FIGURE 8.28

Response of speed control system to a unit step command for different gains.

For this autopilot both the change in velocity and the acceleration are used in the feedback path. The feedback path transfer function is assumed to be of the form that follows:

$$H(s) = 10s + 1$$

The loop transfer function, $G(s)H(s)$, follows:

$$G(s)H(s) = \frac{3.8k_a(s + 0.1)}{(s + 10)(s^2 + 0.039s + 0.053)}$$

The root locus plot of the loop transfer function is shown in Figure 8.27.

Figure 8.28 shows the response of the speed control system to a unit step for several different values of the amplifier gain, k_a . The three gains are indicated on Figure 8.27. Note that for a gain corresponding to a damping ratio of 0.707 the response is very fast but there is a steady-state error. On the other hand, the steady-state error can be reduced by increasing the gain. However, larger gains mean a lower damping ratio and the response has a larger overshoot. To improve the performance of this system an additional compensator should be considered.

8.5

STABILITY AUGMENTATION

Another application of automatic devices is to provide artificial stability for an airplane that has undesirable flying characteristics. Such control systems are commonly called stability augmentation systems (SAS).

As we showed earlier, the inherent stability of an airplane depends on the aerodynamic stability derivatives. The magnitude of the derivatives affects both the damping and frequency of the longitudinal and lateral motions of an airplane. Furthermore, it was shown that the stability derivatives were a function of the airplane's aerodynamic and geometric characteristics. For a particular flight regime it would be possible to design an airplane to possess desirable flying qualities. For example, we know that the longitudinal stability coefficients are a function of the horizontal tail volume ratio. Therefore we could select a tail size and or location so that C_{m_q} and C_{m_a} provide the proper damping and frequency for the short-period mode. However, for an airplane that will fly throughout an extended flight envelope, one can expect the stability to vary significantly, owing primarily to changes in the vehicle's configuration (lowering of flaps and landing gear) or Mach and Reynolds number effects on the stability coefficients. Because the stability derivatives vary over the flight envelope, the handling qualities also will change. Obviously, we would like to provide the flight crew with an airplane that has desirable handling qualities over its entire operational envelope. This is accomplished by employing stability augmentation systems.

EXAMPLE PROBLEM 8.5. To help understand how a stability augmentation system works, we shall consider the case of an airplane having poor short-period dynamic characteristics. In our analysis we assume that the aircraft has only one degree of freedom—a pitching motion about the center of gravity. The equation of motion for a constrained pitching motion as developed in Chapter 4 is

$$\ddot{\theta} - (M_q + M_a)\dot{\theta} + M_a\theta = M_\delta\delta$$

The damping ratio and undamped natural frequency are given by

$$\zeta_{sp} = -(C_{m_q} + C_{m_a})\frac{\rho u_0 S \bar{c}^2}{4I_y}/(2\omega_{nsp})$$

$$\omega_{nsp}^2 = -C_{m_a}\frac{\rho u_0^2 S \bar{c}}{2I_y}$$

If the aerodynamic and inertial characteristics of a business jet during cruise are such that the preceding equations have the numerical values

$$\ddot{\theta} + 0.071\dot{\theta} + 5.49\theta = -6.71\delta_e$$

then the damping ratio and frequency are given by

$$\zeta_{sp} = 0.015 \quad \omega_{nsp} = 2.34 \text{ rad/s}$$

For these short-period characteristics the airplane has poor flying qualities. On examining the flying quality specification, we see that to provide level 1 flying qualities the short-period damping must be increased so that $\zeta_{sp} > 0.3$.

One means of improving the damping of the system is to provide rate feedback, as illustrated in Figure 8.29. This type of system is called a pitch rate damper. The stability augmentation system provides artificial damping without interfering with the pilot's control input. This is accomplished by producing an elevator deflection in proportion to the pitch rate and adding it to the pilot's control input:

$$\delta_e = \delta_{ep} + k\dot{\theta}$$

where δ_{ep} is that part of the elevator deflection created by the pilot. A rate gyro is used to measure the pitch rate and creates an electrical signal that is used to provide elevator deflections. If we substitute the expression for the elevator angle back into the equation of motion, we obtain

$$\ddot{\theta} + (0.071 + 6.71k)\dot{\theta} + 5.49\theta = -6.71\delta_{ep}$$

Comparing this equation with the standard form of a second-order system yields

$$2\zeta\omega_n = (0.071 + 6.71k) \quad \text{and} \quad \omega_n^2 = 5.49$$

The short-period damping ratio is now a function of the gyro gain k and can be selected so that the damping ratio will provide level 1 handling qualities. For example, if k is chosen to be 0.2, then the damping ratio $\zeta = 0$.

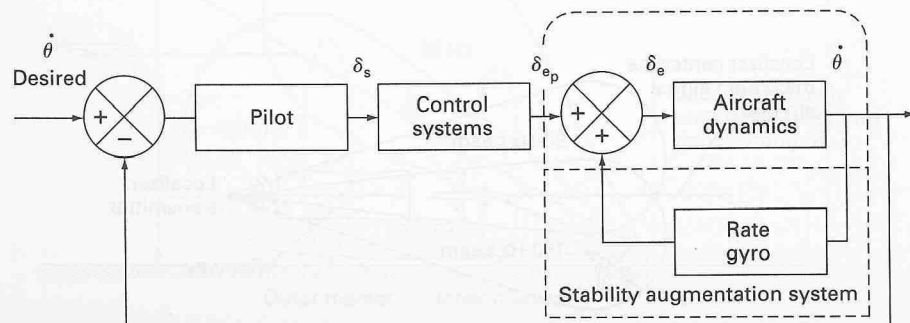


FIGURE 8.29

Stability augmentation system using pitch rate feedback.

8.6 INSTRUMENT LANDING

With the advent of the instrument landing system (ILS), aircraft became able to operate safely in weather conditions with restricted visibility. The instrument landing system is composed of ground-based signal transmitters and onboard receiving equipment. The ground-based equipment includes radio transmitters for the localizer, glide path, and marker beacons. The equipment on the airplane consists of receivers for detecting the signals and indicators to display the information.

The basic function of the ILS is to provide pilots with information that will permit them to guide the airplane down through the clouds to a point where the pilot re-establishes visual sighting of the runway. In a completely automatic landing, the autopilot guides the airplane all the way down to touchdown and roll out.

Before addressing the autoland system, we briefly review the basic ideas behind the ILS equipment. To guide the airplane down toward the runway, the guidance must be lateral and vertical. The localizer beam is used to position the aircraft on a trajectory so that it will intercept the centerline of the runway. The transmitter radiates at a frequency in a band of 108–112 MHz. The purpose of this beam is to locate the airplane relative to a centerline of the runway. This is accomplished by creating azimuth guidance signals that are detected by the onboard localizer receiver. The azimuth guidance signal is created by superimposing a 90-Hz signal directed toward the left and a 150-Hz signal directed to the right on the carrier signal. Figure 8.30 shows an instrument landing localizer signal. When the aircraft is flying directly along the projected extension of the runway centerline, both superimposed signals are detected with equal strength. However, when the aircraft deviates say to the right of centerline, the 150-Hz signal is stronger. The receiver in the cockpit detects the difference and directs the pilot to fly the aircraft to the left by way of a vertical bar on the ILS indicator that shows the airplane to the right of the runway. If the airplane deviates to the left, the indicator will deflect the bar to the left of the runway marker.

The glide path or glide slope beam is located near the runway threshold and radiates at a frequency in the range 329.3–335.0 MHz. Its purpose is to guide the aircraft down a predetermined descent path. The glide slope is typically an angle

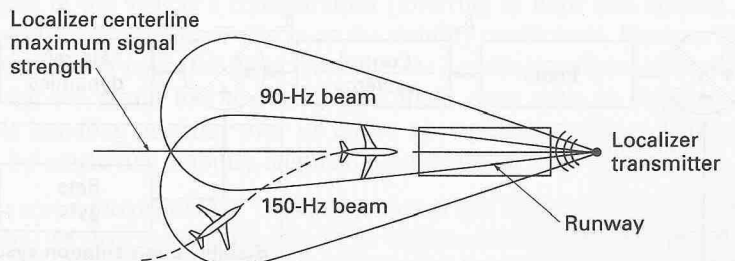


FIGURE 8.30
A localizer beam system.

of 2.5–3° to the horizontal. Figure 8.31 shows a schematic of the glide path beam. Note that the glide path angle has been exaggerated in this sketch. As in the case of the localizer, two signals are superimposed on the carrier frequency to create an error signal if the aircraft is either high or low with respect to the glide path. This usually is indicated by a horizontal bar on the ILS indicator that moves up or down with respect to the glide path indicator. The marker beacons are used to locate the aircraft relative to the runway. Two markers are used. One, located 4 nautical miles from the runway, is called the outer marker. The second, or inner, marker is located 3500 ft from the runway threshold. The beams are directed vertically into the descent path at a frequency of 75 MHz. The signals are coded, and when the airplane flies overhead the signals are detected by an onboard receiver. The pilot is alerted to the passage over a marker beacon by both an audio signal and visual signal. The audio signal is heard over the aircraft's communication system and the visual signal is presented by way of a colored indicator light on the instrument panel.

In flying the airplane in poor visibility, the pilot uses the ILS equipment in the following manner. The pilot descends from cruise altitude under direction of ground control to an altitude of approximately 1200 ft above the ground. The pilot then is vectored so that the aircraft intercepts the localizer at a distance of at least 6 nautical miles from the runway. The pilot positions the airplane using the localizer display so that it is on a heading toward the runway centerline. When the aircraft approaches the outer marker, the glide path signal is intercepted. The aircraft is placed in its final approach configuration and the pilot flies down the glide path slope. The pilot follows the beams by maneuvering the airplane so that the vertical and horizontal bars on the ILS indicator show no deviation from the desired flight path. The ILS system does not guide the aircraft all the way to touchdown. At some point during the approach the pilot must look away from the instruments and outside the window to establish a visual reference for the final portion of the

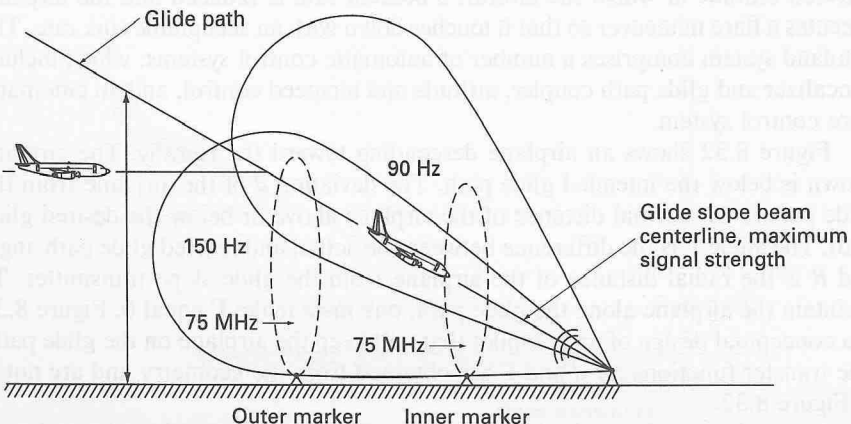


FIGURE 8.31
A glide slope beam system.

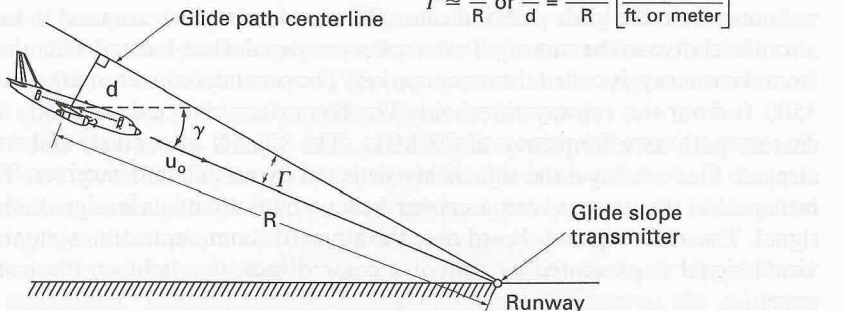


FIGURE 8.32
An airplane displaced from the glide path.

landing. The pilot may take 5 or 6 seconds to establish an outside visual reference. Obviously the pilot must do this at sufficient altitude and distance from the runway so that if the runway is not visible the pilot can abort the landing. This gives rise to a “decision height,” which is a predetermined height above the runway that the pilot cannot go beyond without visually sighting the runway.

The ILS as outlined in the previous paragraphs is an integral part of a fully automatic landing system. To be able to land an airplane with no visual reference to the runway requires an automatic landing system that can intercept the localizer and glide path signals, then guide the airplane down the glide path to some pre-selected altitude at which the aircraft’s descent rate is reduced and the airplane executes a flare maneuver so that it touches down with an acceptable sink rate. The autoland system comprises a number of automatic control systems, which include a localizer and glide path coupler, attitude and airspeed control, and an automatic flare control system.

Figure 8.32 shows an airplane descending toward the runway. The airplane shown is below the intended glide path. The deviation d of the airplane from the glide path is the normal distance of the airplane above or below the desired glide path. The angle Γ is the difference between the actual and desired glide path angle and R is the radial distance of the airplane from the glide slope transmitter. To maintain the airplane along the glide path, one must make Γ equal 0. Figure 8.33 is a conceptual design of an autopilot that will keep the airplane on the glide path. The transfer functions for d and Γ are obtained from the geometry and are noted in Figure 8.32.

As the airplane descends along the glide path, its pitch attitude and speed must be controlled. This again is accomplished by means of a pitch displacement and speed control autopilot. The pitch displacement autopilot would be conceptually

$$d = u_0 \sin \gamma = u_0 \gamma$$

$$\frac{\gamma}{d} = \frac{u_0}{57.3s} \left[\begin{array}{l} \text{degrees} \\ \text{ft. or meter} \end{array} \right]$$

$$\tan \Gamma = \frac{d}{R}$$

$$\Gamma \approx \frac{d}{R} \text{ or } \frac{\Gamma}{d} = \frac{57.3}{R} \left[\begin{array}{l} \text{degrees} \\ \text{ft. or meter} \end{array} \right]$$

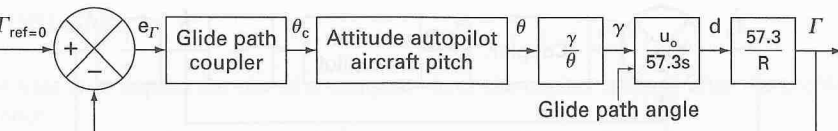


FIGURE 8.33
An automatic glide path control system.

the same as the one discussed earlier in this chapter. Figure 8.34 shows an automatic control system that could be used to maintain a constant speed along the flight path. The difference in flight speed is used to produce a proportional displacement of the engine throttle so that the speed difference is reduced. The component of the system labeled compensation is a device incorporated into the design so that the closed-loop system can meet the desired performance specifications. Finally, as the airplane gets very close to the runway threshold, the glide path control system is disengaged and a flare maneuver is executed. Figure 8.35 illustrates the flare maneuver just prior to touchdown. The flare maneuver is needed

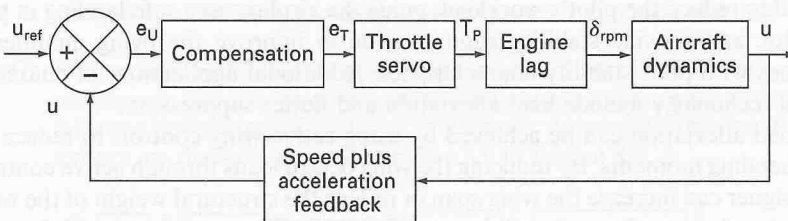


FIGURE 8.34
An automatic speed control system.

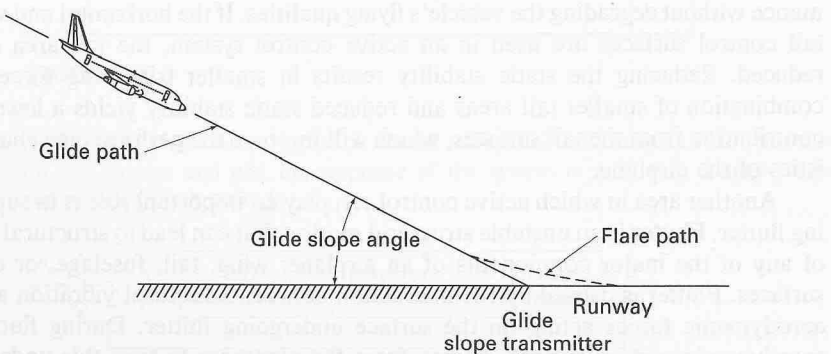
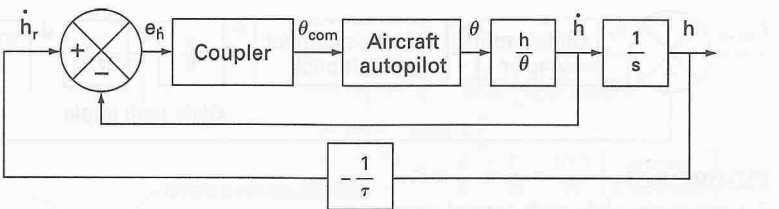


FIGURE 8.35
A flare maneuver.

**FIGURE 8.36**

An automatic flare control system.

to decrease the vertical descent rate to a level consistent with the ability of the landing gear to dissipate the energy of the impact at landing. An automatic flare control system is shown in Figure 8.36. A detailed discussion of the autoland system is provided by Blakelock [8.3].

8.7

SUMMARY

In this chapter we examined briefly the use of an automatic control system that can be used to reduce the pilot's workload, guide the airplane to a safe landing in poor visibility, and provide stability augmentation to improve the flying qualities of airplanes with poor stability characteristics. Additional applications of automatic control technology include load alleviation and flutter suppression.

Load alleviation can be achieved by using active wing controls to reduce the wing-bending moments. By reducing the wing design loads through active controls, the designer can increase the wing span or reduce the structural weight of the wing. Increasing the span for a given wing area improves the aerodynamic efficiency of the wing; that is, it increases the lift-to-drag ratio. The improvement in aerodynamic efficiency and the potential for lower wing weight result in better cruise fuel efficiency.

Stability augmentation systems also can be used to improve airplane performance without degrading the vehicle's flying qualities. If the horizontal and vertical tail control surfaces are used in an active control system, the tail area can be reduced. Reducing the static stability results in smaller trim drag forces. The combination of smaller tail areas and reduced static stability yields a lower drag contribution from the tail surfaces, which will improve the performance characteristics of the airplane.

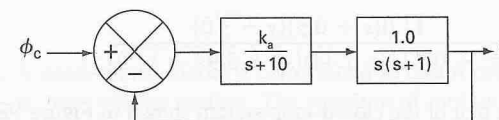
Another area in which active control can play an important role is in suppressing flutter. Flutter is an unstable structural motion that can lead to structural failure of any of the major components of an airplane: wing, tail, fuselage, or control surfaces. Flutter is caused by the interaction between structural vibration and the aerodynamic forces acting on the surface undergoing flutter. During flutter the aerodynamic surface extracts energy from the airstream to feed this undesirable motion. An automatic control system incorporating active controls can be designed to prevent flutter from occurring by controlling the structural vibration.

PROBLEMS

Problems that require the use of a computer have the capital letter C after the problem number.

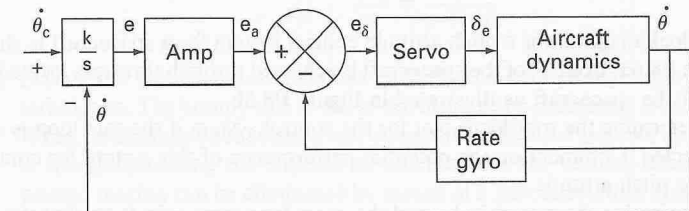
- 8.1(C).** A roll control system is shown in Figure P8.1. Sketch the root locus diagram for this system.

- Determine the value of the gain, k , so that control system has a damping ratio of $\zeta = 0.707$.
- What is the steady-state error for a step and ramp input?
- Sketch the response of the control system to a 5° step change in bank angle command.
- Repeat this problem using control synthesis software such as MATLAB.

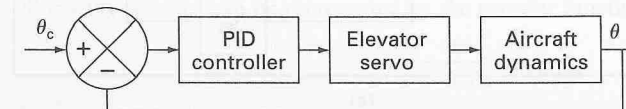
**FIGURE P8.1**

- 8.2(C).** Use a rate feedback inner loop to improve the transient response of the control system in Problem 8.1. The system damping ratio is to remain at $\zeta = 0.707$.

- 8.3(C).** For the pitch rate feedback control system shown in Figure P8.3, determine the gain necessary to improve the system characteristics so that the control system has the following performance: $\zeta = 0.3$, $\omega_n = 2.0 \text{ rad/s}$. Assume that the aircraft characteristics are the same as given in Figure 8.9 in Section 8.4.

**FIGURE P8.3**

- 8.4(C).** A simplified pitch control system is shown in Figure P8.4. Design a PID controller for this system and plot the response of the system to a 5° step change in the commanded pitch attitude.

**FIGURE P8.4**

PID	$k_p + \frac{k_i}{s} + k_d s$
Elevator servo	$-\frac{10}{s+10}$
Aircraft dynamic	$\frac{-3}{s^2 + 3s + 4.0}$

8.5(C). The Wright Flyer was statically and dynamically unstable. However, because the Wright brothers incorporated sufficient control authority into their design they were able to fly their airplane successfully. Although the airplane was difficult to fly, the combination of the pilot and airplane could be a stable system. In [8.5] the closed-loop pilot is represented as a pure gain, k_p , and the pitch attitude to canard deflection is given as follows:

$$\frac{\theta}{\delta_c} = \frac{11.0(s + 0.5)(s + 3.0)}{(s^2 + 0.72s + 1.44)(s^2 + 5.9s - 11.9)}$$

Determine the root locus plot of the closed-loop system shown in Figure P8.5. For what range of pilot gain is the system stable?

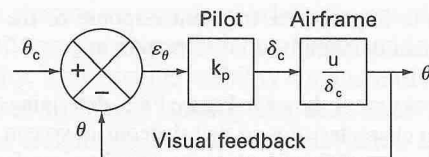


FIGURE P8.5

8.6(C). The block diagram for a pitch attitude control system for a spacecraft is shown in Figure P8.6a. Control of the spacecraft is achieved through thrusters located on the side of the spacecraft as illustrated in Figure P8.6b.

- (a) Determine the root locus plot for the control system if the rate loop is disconnected. Comment on the potential performance of this system for controlling the pitch attitude.
- (b) Determine the rate gain k_{rg} and the outer loop gyro gain k_g so that the system has a damping ratio $\zeta = 0.707$ and a settling time, $t_s = 1.5$ s.

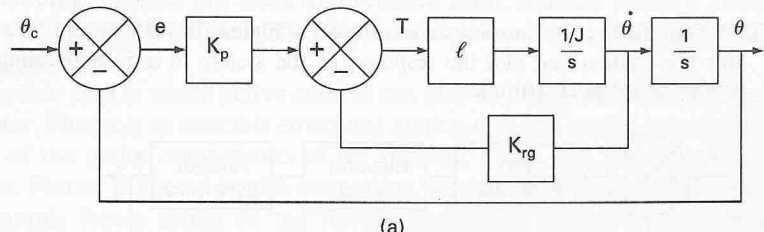


FIGURE P8.6

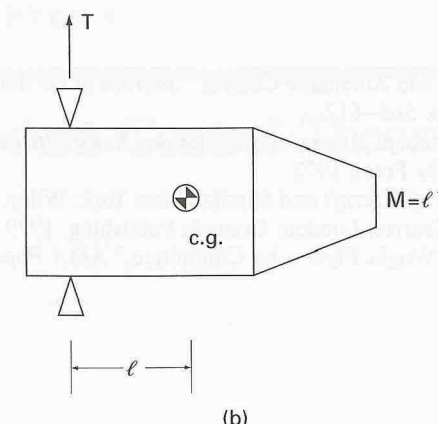


FIGURE P8.6 (continued)

8.7(C). A wind-tunnel model is constrained so that it can rotate only about the z axis; that is, pure yawing motion. The equation of motion for a constrained yawing motion was shown in Chapter 5 to be as follows:

$$\Delta\ddot{\psi} - N_r \Delta\dot{\psi} + N_\beta \Delta\psi = N_\delta \Delta\delta_r$$

where $N_\beta = 2.0 \text{ s}^{-2}$, $N_r = -0.5 \text{ s}^{-1}$ and $N_{\delta_r} = -10 \text{ s}^{-2}$. Design a heading control system so that the model has the following closed-loop performance characteristics:

$$\zeta = 0.6$$

$$t_s \leq 2.5$$

Assume that the rudder servo transfer function can be represented as

$$\frac{\Delta\delta_r}{e} = \frac{k}{s + 10}$$

8.8(C). Every pilot or airline passenger has encountered a rough flight due to atmospheric turbulence. The bumpy ride is due to the airplane encountering a vertical gust field. When an airplane encounters a vertical gust the effective angle of attack of the wing is changed, causing the airplane to accelerate in the vertical direction. This unwanted motion can be eliminated by means of a gust alleviation system. If the wing lift can be controlled, the acceleration due to the gust can be attenuated. One means of controlling the wing lift is by using direct lift controls. Basically, direct lift control surfaces are wing flaps that can be rotated up or down to either decrease or increase the wing lift. Consider a wind-tunnel model constrained to motion in only the vertical direction; that is, pure plunging motion. Also assume that the model is equipped with direct lift flaps. See Example Problem 8.3. Design a control system for the wind-tunnel model so that the vertical velocity is held near 0. Assume the direct lift actuator can be represented by the transfer function

$$\frac{\delta_f}{e} = \frac{k}{s + 10}$$

8.9(C). Design a control system for the wind tunnel model of Problem 8.8 to maintain a constant vertical position in the wind tunnel.

REFERENCES

- 8.1. Bollay, W. "Aerodynamic Stability and Automatic Control." *Journal of the Aeronautical Sciences*, 18, no. 9 (1951), pp. 569–617.
- 8.2. McRuer, D.; I. Ashkenas; and D. Graham. *Aircraft Dynamics and Automatic Control*, Princeton, N.J.: Princeton University Press, 1973.
- 8.3. Blakelock, J. H. *Automatic Control of Aircraft and Missiles*. New York: Wiley, 1991.
- 8.4. Pallett, E. H. J. *Automatic Flight Control*, London: Granada Publishing, 1979.
- 8.5. Culick, F. E. C. "Building a 1903 Wright Flyer—by Committee," *AIAA Paper 88-0094*, 1988.

CHAPTER 9

Modern Control Theory

9.1 INTRODUCTION

In Chapters 7 and 8, the design of feedback control systems was accomplished using the root locus technique and Bode methods developed by Evans and Bode, respectively. These techniques are very useful in designing many practical control systems. However, the design of a control system using either of the techniques essentially is by trial and error. The major advantage of these design procedures is their simplicity and ease of use. This advantage disappears quickly as the complexity of the system increases.

With the rapid development of high-speed computers during the recent decades, a new approach to control system design has evolved. This new approach, commonly called modern control theory, permits a more systematic approach to control system design. In modern control theory, the control system is specified as a system of first-order differential equations. By formulating the problem in this manner, the control system designer can fully exploit the digital computer for solving complex control problems. Another advantage of modern control theory is that optimization techniques can be applied to design optimal control systems. To comprehend this theory fully one needs to have a good understanding of matrix algebra; a brief discussion of matrix algebra is included in Appendix C.

It is not possible in a single chapter to present a thorough discussion of modern control theory. Our purpose is to expose the reader to some of the concepts of modern control theory and then apply the procedures to the design of aircraft autopilots. It is hoped that this brief discussion will provide the reader with an appreciation of modern control theory and its application to the design of aircraft flight control systems. Additional background material on modern control theory can be found in the references included at the end of this chapter [9.1–9.5].